An MRI method for parcellating the human striatum into matrix and striosome compartments *in vivo*

JL Waugh[a,b,d,e,h,i,*], **AAO Hassan**[a], **JK Kuster**[e,f,h,k], **JM Levenstein**[e,h,l,m], **SK Warfield**[c,d], **N Makris**[d,g,h,j], **N Brüggemann**[n,o,l], **N Sharma**[d,i,1], **HC Breiter**[f,p,1], **AJ Blood**[e,f,h,j]

[a]Division of Pediatric Neurology, Department of Pediatrics, University of Texas Southwestern, Dallas, TX, United States

[b]Division of Child Neurology, University of Texas Southwestern, Dallas, TX, United States

[c]Department of Radiology, United States

[d]Boston Children's Hospital, Harvard Medical School, Boston, MA, United States

[e]Mood and Motor Control Laboratory, Boston, MA, United States

[f]Laboratory of Neuroimaging and Genetics, United States

[g]Center for Morphometric Analysis, United States

[h]Martinos Center for Biomedical Imaging, United States

[i]Massachusetts General Hospital, Charlestown, MA, United States

[j]Departments of Neurology and Psychiatry, Charlestown, MA, United States

[k]Rheumatology, Allergy and Immunology Section, Massachusetts General Hospital, Boston, MA, United States

[l]Yale School of Medicine, New Haven, CN, United States

[m]Wellcome Centre for Integrative Neuroimaging, National Institutes of Health, Bethesda, MD, United States

[n]Department of Neurology, University of Oxford, Oxford, United Kingdom

[o]Institute of Neurogenetics, University of Lübeck, Lübeck, Germany

[*]Corresponding author at: Division of Pediatric Neurology, Department of Pediatrics, University of Texas Southwestern, Dallas, TX, United States. jeff.waugh@utsouthwestern.edu (J. Waugh).
[1]These authors contributed equally to this work.

[p]Warren Wright Adolescent Center, Department of Psychiatry and Behavioral Sciences, Northwestern University Feinberg School of Medicine, Chicago, IL, United States

Abstract

The mammalian striatum is comprised of intermingled tissue compartments, matrix and striosome. Though indistinguishable by routine histological techniques, matrix and striosome have distinct embryologic origins, afferent/efferent connections, surface protein expression, intra-striatal location, susceptibilities to injury, and functional roles in a range of animal behaviors. Distinguishing the compartments previously required post-mortem tissue and/or genetic manipulation; we aimed to identify matrix/striosome non-invasively in living humans. We used diffusion MRI (probabilistic tractography) to identify human striatal voxels with connectivity biased towards matrix-favoring or striosome-favoring regions (determined by prior animal tract-tracing studies). Segmented striatal compartments replicated the topological segregation and somatotopic organization identified in animal matrix/striosome studies. Of brain regions mapped in prior studies, our human brain data confirmed 93% of the compartment-selective structural connectivity demonstrated in animals. Test-retest assessment on repeat scans found a voxel classification error rate of 0.14%. Fractional anisotropy was significantly higher in matrix-like voxels, while mean diffusivity did not differ between the compartments. As mapped by the Talairach human brain atlas, 460 regions were significantly biased towards either matrix or striosome. Our method allows the study of striatal compartments in human health and disease, *in vivo*, for the first time.

Keywords

Striatal compartments; Striosome; Patch; Matrix; Classification targets tractography; Diffusion MRI

1. Introduction

The mammalian striatum is divided into distinct but interdigitated compartments known as the matrix and striosome (aka patch). Distinguishing between the two compartments is impossible with routine histological stains, and in adults they have indistinguishable resting electrophysiologic profiles (Kawaguchi et al., 1989; Smith et al., 2016; McGregor et al., 2019). However, the two compartments are readily identified using immunohistochemical methods, with more than sixty proteins (Crittenden and Graybiel, 2011; Mandemakers et al., 2012; West et al., 2014; Morigaki and Goto, 2015) differentially enriched in one compartment. Matrix and striosome are both comprised of medium spiny neurons (MSNs), but the two populations migrate to the striatum at different times (McGregor et al., 2019; Graybiel and Hickey, 1982; van der Kooy and Fishell, 1987), they have distinct patterns of afferent and efferent connectivity (reviewed herein), relatively-segregated vascular supplies (Feekes and Cassell, 2006), and have been hypothesized to fill opposing roles in models of learning (Joel et al., 2002), reward and addiction (White and Hiroi, 1998; Salinas et al., 2016), and motor action selection (Stephenson-Jones et al., 2013). In the human striatum (Graybiel and Ragsdale, 1978; Faull et al., 1989; Holt et al., 1997), matrix and striosome follow an organizational pattern seen from rodents to primates: striosomes are concentrated

in the medial, rostral, and ventral striatum, while matrix dominates in the lateral, caudal, and dorsal striatum (Graybiel and Ragsdale, 1978; Goldman-Rakic, 1982; Donoghue and Herkenham, 1986; Ragsdale and Graybiel, 1990; Desban et al., 1993; Eblen and Graybiel, 1995).

The requirement that tissue be *ex vivo* (for fixation and immunohistochemical staining) to distinguish striatal compartments has limited the study of human diseases with prominent striatal pathologies. More than ten human diseases have been hypothesized to have a matrix- or striosome-specific pattern of injury (Crittenden and Graybiel, 2011), with selective involvement of one striatal compartment identified on post-mortem assessment or inferred based on the suspected functional roles of each compartment. For these neurodegenerative diseases, brain tissue from early symptomatic phases of the disease is scarce, making etiopathological-clinical correlations difficult. One exception is Huntington disease: relatively-selective striosomal degeneration yields mood-dominated symptoms, while mixed matrix-striosome degeneration is associated with primarily motor symptoms (Tippett et al., 2007). These post-mortem assessments are supported by indirect evidence from *in vivo* diffusion MRI in Huntington disease, with higher depression and apathy measures in individuals with larger abnormalities in corticostriate projections from areas that, in animals, favor connectivity with striosomes (Sprengelmeyer et al., 2014; De Paepe et al., 2019). Similarly, we recently demonstrated that diffusion connectivity with striosome-favoring cortical regions is elevated in X-linked Dystonia Parkinsonism (XDP) (Blood et al., 2017), a disorder with relatively-selective striatal atrophy (Crittenden and Graybiel, 2011). However, neither of these disease-focused approaches attempted to distinguish striatal compartments. Indeed, for all diseases with hypothesized compartment-selective injury, it has been impossible to directly assess the striatal compartments *in vivo,* or to track compartment-specific injury longitudinally through the course of disease.

Abnormal matrix or striosome function has also been hypothesized to underlie brain-based diseases that lack overt neuropathology. In DOPA-responsive dystonia (DRD), both human (Segawa et al., 2013) and animal (Sato et al., 2008) histology demonstrates a striosome-specific reduction in dopamine synthesis at nigrostriatal terminals. Disorders of compulsion and pathological habit formation, such as obsessive-compulsive disorder, tic disorders, stereotypies, and addictions to food or drugs, may also relate to abnormalities in striosome function (Eblen and Graybiel, 1995; Crittenden et al., 2017; Jenrette et al., 2019; Nadel et al., 2020). Associations between one striatal compartment and these non-degenerative diseases are inferential, merging animal histochemistry and clinical observations in humans. These diseases are common, but are generally non-fatal – tissue available for neuropathological assessment is typically decades removed from symptom onset, limiting our understanding of where and how they begin.

The dimensions of striosomes in coronal sections (0.36×1.0 mm for macaque (Mikula et al., 2009), approximately 0.5×1.25 mm for humans (Graybiel and Ragsdale, 1978; Holt et al., 1997)) limit their assessment by structural brain imaging. At the standard resolution for 3 Tesla (3T) structural MRI (1 mm^3), striosomes are subject to partial volume averaging and loss of precision. At 7T, using research MRI protocols (Lusebrink et al., 2017), structural imaging can achieve a resolution of 0.25^3 mm – but such scans required 8 h, limiting

use in patients. Even at sub-millimeter resolution, however, matrix and striosomes may be indistinguishable on structural scans, since they have no recognized macroscale differences in tissue composition. Region of interest approaches are also insufficiently precise to segregate the two compartments, as matrix and striosome are interdigitated, even in zones relatively enriched in striosomes, and the precise location of striosomes varies between individuals.

Given these limitations, we set out to distinguish matrix and striosomes in humans based on their patterns of structural connectivity, using probabilistic tractography derived from diffusion MRI. A wealth of histological literature, utilizing injected tracers in animals, provided us with diffusion targets whose patterns of connectivity were segregated between matrix and striosomes. We developed this MRI method in one cohort of healthy individuals, and then tested it in two independent cohorts, for a combined group of 122 healthy adults. This method allowed us to non-invasively assess the striatum at a compartment level *in vivo*, a first in any species.

2.   Methods

2.1.   Prior literature utilizing injectable tract tracers

Injectable tract tracers in animals have been used since the early 1980s to identify patterns of connectivity between injected targets and the matrix and striosome compartments. We identified publications that utilized injected tract tracing techniques to study striatal compartment connectivity using serial Pubmed searches with "striatum inject" and one of the following terms: matrix, striosome, patch, or compartment. We sought to identify any study that characterized connectivity with the striatum at the compartment level, including those that utilized tritiated amino acids, biocytin, cholera toxin B, FluoroGold™, horseradish peroxidase, and *Phaseolus vulgaris*-leucoagglutinin. We included all regions with data from at least two animals (Smith et al., 2016; McGregor et al., 2019; Goldman-Rakic, 1982; Donoghue and Herkenham, 1986, 20; Eblen and Graybiel, 1995; Gerfen, 1984, 1989; Malach and Graybiel, 1986; Berendse et al., 1988; Desban et al., 1989; Jimenez-Castellanos and Graybiel, 1989; Langer and Graybiel, 1989; Gimenez-Amaya and Graybiel, 1990; Ragsdale and Graybiel 1991; Sadikot et al., 1992; Parthasarathy et al., 1992; Ebrahimi et al., 1992; Rajakumar et al., 1993; Flaherty and Graybiel, 1993; Haber et al., 1995; Desban et al., 1995; Lopez-Figueroa et al., 1995; Deschenes et al., 1996; Inase et al., 1996; Kincaid and Wilson, 1996; Funaki et al., 1998; Nisenbaum et al., 1998; Reep et al., 2003; Cheatwood et al., 2005; Avendano et al., 2006; Kamishina et al., 2008; Day-Brown et al., 2010; Unzai et al., 2015) These searches and review of references from these articles yielded 42 regions in which connectivity was reported at the compartment level (Supplemental Table 1).

2.2.   Participants

We utilized three distinct cohorts of healthy volunteers, totaling 123 Participants, all scanned at an MRI field strength of 3T (scan session details per cohort are described below). Striatal segmentation in one subject was judged to be unreliable (unmeasurable connectivity for multiple tested regions) so was excluded from further analysis, yielding a final combined cohort of 122 participants. These participants have been described previously (Perlis et

al., 2008; Kim et al., 2010; Blood et al., 2012; Waugh et al., 2016; Bruggemann et al., 2016; Hanssen et al., 2018; Waugh et al., 2019), but none have been previously assessed via the methods described here. The mean age of this cohort was 35.0 years (range: 18–74). One hundred ten participants were right-handed, ten were left-handed, and two were ambidextrous. Fifty-eight participants were female; sixty-four were male. These individuals were recruited as control participants for three distinct disease-related protocols, each of which was approved by the Institutional Review Board for the respective institution. All participants screened negative for any prior neurologic or psychiatric history. Participants were provided with printed materials describing the respective research protocol and were encouraged to ask questions regarding the study. We obtained written consent for all participants. All research was conducted in accordance with the principles in the Declaration of Helsinki.

Cohort A: Thirty-six participants were scanned at the MGH Martinos Center for Biomedical Imaging (Charlestown, MA, USA).[64, 65, 68] Their self-identified ethnic makeup was: 3 African American; 5 Asian; 27 Caucasian; 1 multiracial. The mean age of this cohort was 40.5 years (range: 18–74). Thirty-three participants were right-handed, two were left-handed, and one was ambidextrous. Twenty participants were female; 16 were male. Thirty-one participants were scanned on a Siemens Tim Trio MRI; five participants were scanned on a Siemens Allegra MRI. This cohort was utilized to establish the tractographic method described below; this method was then tested using Cohorts B and C. Fourteen of these participants were scanned a second time, always utilizing the same MRI scanner for both acquisitions. We compared voxel location between the two scans to assess the longitudinal validity of the technique.

Cohort B: Twenty-six participants were scanned at the University of Lübeck (Lübeck, Germany). (Bruggemann et al., 2016; Hanssen et al., 2018) All participants were ethnic Filipinos. The mean age of this cohort was 35.7 years (range: 19–53). Twenty-five participants were right-handed, and one was ambidextrous. Seven participants were female; 19 were male. Twenty-three were scanned on a Philips Achieva MRI; 3 were scanned on a Philips Ingenia MRI.

Cohort C: Sixty-one participants were scanned at the MGH Athinoula A. Martinos Center for Biomedical Imaging (Charlestown, MA, USA). (Perlis et al., 2008; Kim et al., 2010) Their self-identified ethnic makeup was: 6 African American; 5 Asian; 48 Caucasian; 2 Native American. The mean age of this cohort was 31.5 years (range: 19–54). Fifty-three participants were right-handed; 8 were left-handed. Thirty-one participants were female; 30 were male. All participants were scanned on the same Siemens Tim Trio MRI described for Cohort A.

2.3. MRI acquisition

Participants in all cohorts were imaged using 3T high-resolution whole brain diffusion tensor imaging (DTI) sequences with a resolution of 2 mm isotroopic, and 32-channel head coils. We acquired Cohorts A and C utilizing the following parameters: repetition time (TR) = 8 s; echo time (TE) = 83 ms; slice thickness = 2 mm; 60 slices total,

six averages; 60 noncolinear directions; with b-value = 700 s/mm^2, and one image with b-value = 0 s/mm^2. DTI scans in each subject were acquired using auto-align software (van der Kouwe et al., 2005) to normalize brain image slice orientation between participants and across scan sessions. We acquired Cohort B utilizing the following parameters: TR = 7582 ms; TE = 60 ms; slice thickness = 2 mm; 70 slices total; 32 noncolinear directions, with b-value = 1000 s/mm^2. Preprocessing and tractography steps were carried out in that participant's native DTI space. To increase the signal to noise ratio, data were upsampled to that individual's MPRAGE T1 image (172 slices, 1 mm^3 isometric) using the FSL tools *flirt/fnirt* and configuration file FA_2_FMRIB58_1 mm.cnf. For all cohorts, we collected DTI and T1-MPRAGE images in the same scan session.

2.4. Regions of interest and exclusion masks

Regions of interest (ROIs) were manually segmented on the MNI152_T1_1 mm standard brain using the atlas of Talairach and Tournoux (Talairach and Tournoux 1998) to produce anatomically correct segmentations, and then compared with the FMRIB58_FA_1 mm standard brain to ensure an anatomically-robust match. All standard space ROIs were transformed into each subject's native space to act as seed, target, or exclusion masks for probabilistic tractography. The primary motor cortex (PMC) segmentation utilized previously-defined anatomical landmarks. (White et al., 1997; Picard and Strick, 2001; Chouinard and Paus, 2006) The striatal segmentation did not include the tail of the caudate beyond the caudal-most extent of the putamen, as our prior experience suggested that the small cross-sectional area of the caudate tail in axial planes is difficult for successful automated registration in 2 mm isotropic images. A midline exclusion mask, which blocked all interhemispheric projections (including mis-tracked interhemispheric streamlines) and restricted subsequent analyses to the ipsilateral hemisphere, was 3 voxels wide (in the x dimension) and was centered on the sagittal plane. Readers should note that projections from cortex to striatum, and from thalamus to striatum, are unidirectional. However, the streamlines of probabilistic tractography are agnostic to directionality, sampling both anterograde and retrograde relative to the direction of action potential propagation. Therefore, seed volumes placed in cortex or striatum (if placed somatotopically) will examine the same set of unidirectional projections.

2.5. Using classification targets tractography to parcellate the striatum

2.5.1. Identifying and testing target regions—From our review of prior animal literature utilizing injectable axonal tracers to assess anterograde and/or retrograde connectivity (Supplemental Table 1) we assembled a group of cortical regions whose pattern of connectivity with the striatum was most likely to segregate between the matrix and striosomal compartments. We first selected candidate regions for potential inclusion into this experimental group using the following criteria: the number of studies that studied the region, and the number of animals injected in those studies (minimum = 2 animals); the strength of discrimination between striatal compartments; the similarity of cortical architecture between the tested species and humans; and the similarity of cortico-striatal connectivity between the tested species and humans. Papers that utilized primates for tract tracing were weighted more heavily than those using non-primate species. From this list of

potential target regions, we assembled competing groups of four matrix-projecting and four striosome-projecting regions.

Given the apparent absence of prior human studies on connectivity between particular gray matter structures and the two striatal compartments, and the inability of injectable tracer studies to allow differing brain regions to "compete" for connectivity, it was unknown which combination of human gray matter structures was optimal for segregating between striosome-like and matrix-like voxels. We tested > 40 iterations of these competing gray matter regions to identify the eight cortical regions we utilized for parcellation of the striatum. Each of these iterations effectively parcellated the striatum into striosome-like and matrix-like voxels; we selected the eight cortical regions (four striosome-favoring, four matrix-favoring) that (1) yielded the greatest distinction between striatal compartments, (2) replicated most-closely the anatomical patterns identified in prior animal (Graybiel, 1978; Goldman-Rakic, 1982; Donoghue and Herkenham, 1986, 20; Desban et al., 1993; Eblen and Graybiel, 1995; Gerfen, 1984; Malach and Graybiel, 1986; Desban et al., 1989) and human (Graybiel, 1978; Faull et al., 1989; Holt et al., 1997) histological studies of striosome and matrix, and (3) produced segmentations whose relative abundance was most-similar to those demonstrated in prior histology experiments. Note that these eight regions were used to validate the method and to suggest regions whose connectivity in humans was potentially even more biased than with these initial eight; descriptions of quantitative tractography (below) used a set of ten cortical and subcortical regions, suggested by the combination of animal and human mapping, that partially overlapped with these initial eight cortical regions.

Testing many iterations of striosome- and matrix-favoring cortical targets allowed us to optimize our parcellation method, but also amplified a potential experimental confound: that the pattern of striatal voxels identified as striosome-like and matrix-like was similar to prior histology studies by chance, not because this method truly distinguished between striatal voxels based on their structural connectivity. To avoid this confound, only Cohort A was utilized to optimize the method. Cohorts B and C were preserved in an untested state until the ideal target regions were firmly established in Cohort A, with no retrospective changes in method permitted. The final methods utilized were identical across Cohorts A–C.

2.5.2.   Parcellating the striatum—Striosome-favoring cortical regions (pregenual anterior cingulate, posterior orbitofrontal, anterior insular cortex, and basolateral amygdala) were added to create a composite target mask. The same was done for matrix-favoring regions (primary sensory, gyrus rectus, supplementary motor area, and primary motor cortex). These composite target masks were necessary to account for two features identified by prior striosome/matrix tracing studies in animals: all tested regions had a blend of striosome-projecting and matrix-projecting neurons, even when the region as a whole favored one striatal compartment (Smith et al., 2016; Gerfen, 1989; Kincaid and Wilson, 1996); preference for one striatal compartment may be topographically limited to a portion of the striatum – e.g., striosome-favoring anteroventrally but indiscriminate posterolaterally (Ragsdale and Graybiel, 1990). By including multiple compartment-favoring regions in each target mask, such compartment-specific and topographic inhomogeneities were minimized by the strength of connectivity across the group of regions.

We performed classification targets tractography (CTT) in native space (utilizing the FSL tool *probtrackx2* (Behrens et al., 2007)) with each hemistriatum as seed, and the ipsilateral striosome-favoring and matrix-favoring composite masks as target. A midline exclusion mask in the sagittal plane assured that all retained projections remained ipsilateral. Separate rounds of tractography were run for left and right hemisphere, for all tractography experiments described here. Tract strength was corrected for path length. *Probtrackx2* utilized the following parameters: curvature threshold = 0.2; steplength = 0.5 mm; number of samples = 5000; number of steps per sample = 2000. Each voxel, in each hemistriatum, for each subject, was assigned a probability (0.0–1.0) of tractographic connectivity with either striosome-favoring or matrix-favoring brain regions, thus generating a probability map of each hemistriatum. Voxels with probability of connection   0.87 (> 1.5 standard deviations above the mean) were defined as matrix-like or striosome-like. We describe these voxels as "-like" for two reasons: first, the diameter of human striosomes in coronal sections is reliably less than 1.25 mm (Holt et al., 1997), so every diffusion voxel (2 mm isotropic) has the potential to include both striosome and matrix elements; second, parcellation identifies voxels that "behave" like either striosome or matrix in their pattern of connectivity, but this should not be conflated with actually identifying clusters of isolated matrix or striosome neurons. Selecting voxels from the tails of the distribution increased the probability that a given voxel (1) included matrix in isolation, or (2) included predominantly, though not entirely, striosome.

We hypothesized that the ratio of matrix:striosomes determined by our diffusion tractography method would correlate with the frequency of matrix and striosomes measured in animal and human histology (Holt et al., 1997; Desban et al., 1993; Mikula et al., 2009; Johnston et al., 1990), approximately 85% matrix and 15% striosome. For each subject we determined the total number of striatal voxels in the tractographic seed mask, the number of voxels in the matrix-like distribution (>0.87), and the number of voxels in the striosome-like distribution (>0.87). As no prior histology studies have reported a left-right asymmetry in the ratio of matrix:striosomes, we did not investigate interhemispheric differences.

In Cohort A, 14 participants were scanned twice, always utilizing the same MRI for both scans. We independently parcellated the striatum for scan1 and scan2, then identified voxels that converted from favoring one compartment to favoring the other compartment. The percentage of parcellated voxels that converted between striatal compartments served as a metric of fidelity for the method.

2.5.3.   Defining striatal masks for quantitative tractography—Probabilistic tractography can be biased by the size of target masks; to accurately quantify the probability of connection with striosome-like and matrix-like voxels, we generated striatal target masks that were very nearly equal in size. Utilizing a fixed probability threshold (i.e., retaining all voxels with   0.90 probability of connection with one set of cortical "bait" regions) yielded masks of highly variable volume. Therefore, we selected from among voxels that had probability of connection   0.55 (ensuring that each candidate voxel had a connectivity bias for one set of cortical targets), starting at the upper limit of the probability distribution and accepting voxels until we reached a volume threshold. In this manner, we assured that each striatal compartment was represented by an equal-sized mask made up of its

most-discriminating voxels. We set the volume threshold at 76 native space voxels. We selected this threshold by starting with the volume of each hemistriatum in the MNI_152_1 mm template brain; we then eliminated the volume that would make up the median 3SD in a normally-distributed volume; we split the remainder across two tails of the distribution; and finally, we converted the residual standard space volume to native space voxels. A volume of 76 voxels therefore represents the fraction of the probability distribution 1.5SD above the mean for each striatal compartment. In some participants, selecting the final voxel for inclusion was compounded by a tie in the probability of connection, even to the seventh significant digit. Therefore, mask sizes ranged from 76 to 78 voxels. Within an individual, the difference in volume between matrix-like and striosome-like masks was negligible: 0.72 voxels, or 0.94% of the mask volume. Given our previously-noted observation that striosome-like voxels will, by virtue of our relatively-large diffusion voxels (2 mm isotropic), always include some fraction of matrix tissue, we hypothesized that identifying striosome-like voxels would require dipping farther into the probability distribution than when identifying matrix-like voxels. To test this hypothesis, for each participant and in each hemisphere we extracted the value (probability of connection to either matrix-favoring or striosome-favoring cortex) of the voxel at the lowest point in the probability distribution that was still included in the matrix-like or striosome-like target mask.

For some participants, the probability of connection for striatal voxels was non-normally distributed. In participants with strong bias toward one category of cortical target, it was occasionally impossible to identify 76 voxels that passed the probability threshold (0.55). In those circumstances, striatal masks for both compartments were set to N, the number of voxels that passed the probability threshold. It is important to note, therefore, that while all striosome-like and matrix-like masks drew only from the "winners" in their distribution, the goal of generating equally-sized target masks required that, in some individuals, the resulting pair of striatal masks differed in their absolute probability of connection. In short, all mask voxels were winners, but some voxels were bigger winners than others. We used these equal-volume striatal masks for all subsequent experiments except those described in Section 2.9.

2.6. Location, diffusion properties, and structural connectivity of matrix-like and striosome-like voxels

Each individual's size-matched striosome-like and matrix-like mask files were used to measure voxel location within the striatum, to extract diffusion metrics in native space, and served as seeds for tractography. We measured the location of each voxel relative to the centroid of the region containing it (caudate or putamen) in the Y-dimension (anterior-posterior axis) and Z-dimension (superior-inferior axis). We extracted fractional anisotropy (FA) and mean diffusivity (MD), averaged across all voxels in the mask. These same binary, equal-volume striosome-like and matrix-like masks were utilized as seed regions for probabilistic tractography. In contrast with the previously-noted iterations of CTT (matrix vs. striosomes), we ran these comparisons in two ways: 1) as open-ended seed-based tractography, without inclusion or waypoint masks and excluding only those regions used as seed masks to parcellate the striatum, and 2) using CTT with only a single target mask that included all cortical gray matter. CTT run in this mode quantifies the streamlines generated

by each seed voxel in a striatal mask. These runs therefore (1) mapped the differences in extent and location of projections between matrix-like and striosome-like seed voxels, and (2) quantified the streamline-generating potential of matrix-like and striosome-like voxels. The streamlines of probabilistic tractography reach most voxels in the brain at some very low probability, with the bulk of the streamlines concentrated in a core projection (Waugh et al., 2019). We removed the lowest-amplitude 25% of voxels and derived the maximum value (peak number of streamlines/voxel), and projection volume (number of voxels occupied by streamlines). For each hemisphere, the volume of streamlines from each striatal compartment and the overlap between those volumes were utilized to calculate the Dice similarity coefficient, as follows:

$$\frac{2 \times (Volume_{Projection\ from\ Striosome\ Seed} \cap Volume_{Projection\ from\ Matrix\ Seed})}{Volume_{Projection\ from\ Sriosome\ Seed} + Volume_{Projection\ from\ Matrix\ Seed}}$$

2.7. Whole-hemisphere tractography with striatal compartment targets

The choice of which cortical regions to utilize for striatal parcellation was informed by the number of prior tract tracing studies that investigated that region, and the number and type of animals utilized in those studies. However, prior researchers chose to study those regions for particular experimental aims, not necessarily to establish the relative strength of compartment-specific connectivity across many regions. Therefore, we utilized an initial iteration of whole-hemisphere tractography to identify regions with the strongest discrimination between striatal compartments, and a second iteration of whole-hemisphere tractography for subsequent quantitative tractography steps.

In our initial parcellation step (Section 2.5.3), striatal voxels served as the seed for tractography. Following striatal parcellation and generation of equal-volume masks for each compartment, we reversed the seed-target relationship, setting equal-volume striosome-like and matrix-like voxels as the targets of CTT with the ipsilateral hemisphere's extrastriate gray matter as seed. To prepare the extrastriate gray matter seed mask, we isolated voxels from the MNI_152_1 mm template brain with intensity between 3500 and 7100. Next, we visually inspected and corrected this segmentation, eliminating stray white matter voxels and adding back any gray matter regions falsely excluded. Finally, we subtracted the volume of all eight cortical regions we had used to parcellate the striatum from the extrastriate gray matter mask volume. We removed these bait volumes to avoid circularity between using these regions to classify striatal voxels and then using those same regions to quantify connectivity with the striatum. We ran each hemisphere independently, with tractography parameters identical to those in Section 2.5.2. We ran N-1 analyses (see Section 2.8) on each of the eight regions in turn to quantify connectivity for regions that were subtracted out of the hemispheric mask volume.

The brain regions with the greatest segregation between striosome-like and matrix-like voxels were identified by visual inspection of the averaged whole-brain-to-striatal-compartments CTT. We identified ten gray matter regions whose (1) mean connectivity with one striatal compartment exceeded 60% for both left and right hemispheres, (2) compartment selectivity was relatively homogenous across the region, and (3) prior tract

tracing studies demonstrated preference for the same striatal compartment. We utilized these ten regions in two distinct approaches to quantify compartment-specific structural connectivity: the N-1 analyses, and regional assessment using standard atlases.

2.8. Removing circularity from connectivity estimates: N-1 analyses

Quantification of regional connectivity with striosome-like vs. matrix-like voxels in the methods described in Section 2.7 suffers from circular logic: the striatum was parcellated using particular cortical regions; those same regions cannot then be utilized for quantifying tractographic connectivity. To overcome this limitation, we performed serial iterations of CTT we describe as N-1 analyses (described in some fields as "leave-one-out" analyses).

The ten regions identified through whole-hemisphere CTT (Section 2.7) whose structural connectivity strongly favored one striatal compartment included five matrix-favoring regions (supplementary motor area, primary motor cortex, primary sensory cortex (Brodmann areas 1–3), the VLc and VPLo thalamic nuclei (combined), and the globus pallidus interna) and five striosome-favoring regions (posterior orbitofrontal cortex, basal operculum, anterior insula, basolateral amygdala, and mediodorsal thalamus). For each region in turn, we used the other nine regions (four favoring the same compartment, five favoring the opposite compartment) to parcellate the striatum. Tractographic connectivity of the elided region with each parcellated striatal compartment could then be assessed with clarity, as the tested region was not used to define the target masks. Prior tract tracing studies have observed that the striosome and matrix targets for particular cortical regions are somatotopically organized (Goldman-Rakic, 1982; Donoghue and Herkenham, 1986, 20; Eblen and Graybiel, 1995; Malach and Graybiel, 1986; Berendse et al., 1988), suggesting that each extrastriate seed regions might identify a slightly different pattern of striosome-like and matrix-like voxels. Therefore, for each subject we created 20 equal-volume pairs of unique striatal masks (2 hemispheres x 10 N-1 parcellations) for quantitative tractography; the mean difference in within-individual mask size (# striosome-like voxels vs. # matrix-like voxels) was 0.39 voxels, 0.51% of the target mask volume (76 voxels).

We performed CTT, utilizing the elided region as seed and the striatal compartments defined by the N-1 regions as targets. Connectivity between each N-1 region and the two ipsilateral equal-volume striatal masks was determined through two parallel methods: first, the mean probability of connection across the seed region (non-zero voxels); second, the number of seed voxels with >87% probability of connection to each target mask (selecting those voxels beyond the central-most 3 standard deviations). These two approaches allowed us to identify both general trends in connection across entire regions, and clusters of higher probability connectivity.

2.9. Regional specificity of striosome connectivity

Prior tract tracing studies observed a somatotopic organization of cortico-striate projections, with a particular cortical region projecting to some, but not all, parts of striosome or matrix. We sought evidence of this specificity in human striosome-like voxels by comparing probability maps between two conditions: when segmented using all of the regions utilized for the N-1 experiments (5 matrix-favoring, 5 striosome-favoring, none left out), and

when segmented using only N-1 regions (5 matrix-favoring, 4 striosome-favoring). The striosome-like probability distribution unique to region A, distinct from that of regions B–E, follows the formula $P_{N-1(A-E)} - P_{N-1(B-E)} = P_{N-1A}$. Simply put, comparing probability distributions between two starting conditions (ten bait regions vs. nine bait regions) defines the contribution of the tenth, left-out region. After generating the striosome-like probability maps for each striosome-favoring N-1 region and hemisphere, we averaged probability maps across the group of 122 participants. We selected for the most highly-enriched voxels using an amplitude threshold to retain the highest 0.1% of voxels. It is notable that this method selects for voxels that have the strongest contribution from a given target region relative to other targets, which will underweight voxels in which strong connectivity is contributed by multiple regions. Among the voxels whose connectivity was strongly influenced by one striosome-favoring region, we assessed the number of striosome-like voxels in four anatomical areas along two dimensions: rostral vs. caudal, divided at the anterior commissure ($y = 129$), and caudate vs. putamen. Note that since this experiment dealt only with striosome-like probability distributions, rather than quantifying extrastriate connectivity, and our interest lay in differential connectivity among striosome-favoring regions, we did not generate equal-volume striatal masks.

2.10. Quantitative whole-hemisphere tractography

The N-1 regions met our goals for parcellating the striatum and were effective as extraction masks for quantifying regional connectivity. However, we recognized that many readers will wish to quantify connectivity to regions more applicable to their own research goals, or in regions that conform to those laid out in common neuroanatomic atlases. We parcellated the striatum using all ten N-1 regions (none left out) and set those equal-volume striatal voxels as targets for CTT, utilizing the whole-hemisphere (excluding white matter and all N-1 regions) as seeds. From these whole-hemisphere probability maps (matrix-favoring and striosome-favoring) we set a minimum threshold ($P > 0.55$) to select only voxels with biased connectivity. We extracted voxels in two ways that parallel two potential methods for applying this method in future studies: first, in an unbounded, whole-hemisphere approach; second, using a region-of-interest approach. As a gross estimate of the amount of extrastriate brain projecting to each compartment, we extracted the ratio of the volume of biased ($P > 0.55$) voxels to total voxels in the whole-hemisphere mask for both matrix-like and striosome-like targets. In addition, we extracted connectivity measures for each subject in standard space using regions of interest from three common brain atlases, the Harvard-Oxford Cortical and Subcortical (Desikan et al., 2006) and the Talairach (Lancaster et al., 2000). We utilized the binarized (maxprobthr25–1 mm) versions of each atlas. For atlas regions that overlapped with our N-1 bait regions we needed to remove circularity, just as we described above for the N-1 analyses (Section 2.8). We tested regions with overlap using separate iterations of CTT, setting an individual atlas label as seed and the corresponding (N-1)-parcellated striatum as target. For example, the Harvard-Oxford precentral gyrus label overlapped with our primary motor cortex mask. Therefore, when we tested the precentral gyrus label we utilized the N-1 striatal masks that were parcellated with primary motor cortex elided from the bait regions. It is important to distinguish atlas-based region-of-interest measures from the N-1 assessments described previously – atlas labels are

often much larger (Harvard-Oxford) or much smaller (Talairach) than our N-1 bait regions, and the two are not equivalent.

The Harvard-Oxford atlas (HOA) segments the brain into large regions, all of which had abundant streamline contacts with our striatal targets. We excluded labels that overlapped with the N-1 regions (to avoid circularity of measurement), labels that duplicated a more specific label in the same atlas (e.g., "Cerebral Cortex"), and labels that were predicted to include both matrix- and striosome-favoring areas based on prior animal literature (e.g., "Thalamus"). We thus included 102 HOA regions (51 left-right pairs) for assessment. In addition to quantifying the volume within each region that favored the dominant compartment (either matrix or striosomes), we quantified the ratio of non-dominant: dominant voxels in each region. This allowed us to assess how many non-dominant voxels were "hidden" within a region that was dominated by connectivity to one striatal compartment.

The Talairach atlas identifies 1105 regions, some of which are quite small and thus generate few or no streamlines that reach the striatum. To reduce the possibility that regional means were driven by scanty data, we excluded regions that had streamline data for less than 1/3 of our participants (ensuring that all regions had data from 41 participants) and excluded regions with fewer than 2.5 supra-threshold voxels for each subject, on average). We also excluded Talairach regions that identified CSF spaces or white matter structures. We thus included 545 Talairach regions for assessment.

We quantified connectivity for each atlas region, in each subject, in two ways: first, the percentage of supra-threshold voxels biased toward the dominant compartment, expressed as the group mean; second, the number of subjects that had "extreme" bias in connectivity (95% of suprathreshold voxels biased toward one compartment), expressed as the ratio of the number of participants with 95% bias ($N_{dominant}:N_{nondominant}$). We compared the regions that had biased striatal compartment connectivity with prior animal tract tracing studies to assess for agreement and to identify areas that had not been assessed previously in animals. It must be noted that atlas labels are not the exact equivalent of Brodmann areas or functionally-defined brain structures, the most common means of reporting location in prior studies (Supplemental Table 1). Translating the anatomical area assessed in animal studies into equivalent atlas labels is therefore imprecise, and these maps should be taken as a first estimate.

2.11. Negative control: tractography utilizing imprecise striatal masks

Striosome-like and matrix-like voxels are situated uniquely within each individual, but are not distributed randomly. To test the hypothesis that voxel-level parcellation is critical to the method, we divided each striatum into two masks, with 2 mm isotropic voxels alternating between the two masks in the XYZ planes; imagine a 3-dimensional chessboard, with the two masks represented by the red or black cubes. We performed CTT as described in Section 2.8, using the noted gray matter regions as seeds and the two indiscriminate striatal masks (red vs. black cubes in our analogy) as targets.

Connectivity between each cortical region and the two indiscriminate striatal masks was determined as in the N-1 analyses above (mean connectivity across the region and number of voxels above threshold), with one exception: enumeration of voxels in this negative control analysis required the use of a lower threshold ($P > 0.50$) than that used in the primary analysis ($P > 0.87$), as in this negative control analysis one third of participants had no voxels reaching the higher threshold.

2.12.   Negative control: tractography utilizing FA-defined striatal voxels as targets for CTT

We found that striosome-like and matrix-like voxels differed in their mean FA value. A potential explanation for this finding is that FA influences the specificity of cortico-striate structural connectivity independent of matrix or striosome identity; if true, our method for parcellating the striatum might be compromised by a parallel influence of FA. To test the hypothesis that the level of structural organization (FA) influenced connectivity with various brain regions, we defined striatal masks by mean FA value rather than by striosome-like and matrix-like patterns of connectivity. Specifically, for each hemistriatum, in each subject, we created a mask volume that matched the mean FA value for striosome-like voxels, and a second mask that matched the mean FA value for matrix-like voxels. These masks had equal volume, as we utilized the same volume targets utilized for striosome-like and matrix-like voxels above: 76–78 voxels per mask. We then set these two FA-defined striatal masks as the classification targets for tractography, and used as seed volumes the four cortical regions that demonstrated the greatest segregation between striosome-like and matrix-like targets: primary motor and sensory cortices (to matrix) and basal operculum and posterior orbitofrontal cortex (to striosome). For each seed volume, we then measured the mean probability of connection to the two target masks.

2.13.   Post-hoc assessment of occipitostriate structural connectivity

Given the potential conflict between our results (human) and those of prior tract tracing studies in rodents, we carried out a secondary analysis of structural connectivity between portions of the occipital cortex and the striatum. We generated seed masks from the Talairach atlas for occipital regions that demonstrated preferential connectivity towards one striatal compartment: Brodmann area 17 (cuneus, BA17) and Brodmann area 18 (lingual gyrus, BA18). We performed CTT with the whole striatum as seed and one occipital Talairach mask as target (tractography parameters as per Section 2.5.2). Rather than generating streamlines or an assessment of differential connectivity, utilizing single targets in this mode generated a simple count at each striatal voxel of the number of streamlines that contacted the target mask. Averaging these striatal maps across our group of 122 subjects, then imposing an amplitude threshold at 50% of the maximum amplitude (Waugh et al., 2019; Phillips et al., 2019), and finally selecting the volume of overlap between BA17- and BA18-specific striatum, allowed us to identify the striatal zone most likely to have structural connectivity with Brodmann areas 17 and 18. Independent left and right hemisphere tractography identified a near-identical zone in the ventral-posterior margin of the putamen, which served as at striatal target mask for subsequent quantitative corticostriate CTT.

To test cortical projections to this zone in the ventral-posterior putamen, we generated a pan-cortical seed mask using the Harvard-Oxford cortical atlas (screened to eliminate any white matter or striatal voxels) with our ventral-posterior putaminal mask as the sole target for CTT. We extracted cortico-striate connectivity in two approaches: first, for every HOA cortical region, to quantify the cortical areas most likely to project to this putaminal zone; second, using the same striosome- and matrix-favoring cortical regions that we previously utilized to parcellate the striatum, to identify whether this putaminal zone generally favors striosome-like or matrix-like connectivity.

2.14. Statistical assessment

All statistical tests were performed using Stata (StataCorp, 2013, Stata Statistical Software: Release 13. College Station, TX).

2.14.1. Relative location of striatal compartments—We assessed the relative location of striosome-like and matrix-like voxels (orientation relative to the caudate or putaminal centroid), independently in the anterior-posterior and superior-inferior axes, using a 4-factor ANOVA (scanner, gender, race/ethnicity, and striatal compartment). Location values were normally distributed and had equal variance between striatal compartments (matrix or striosomes). Categorical factors included the scanner type (manufacturer and model), ethnicity, gender, and striatal compartment. To the best of our knowledge, no interhemispheric differences in matrix and striosome location have been described previously. Therefore, we combined left and right striatal measures in our assessment of location. Using the SME utility developed by the UCLA ATS Statistical Consulting Group (Ender, 2021), we performed post-hoc analysis of simple main effects for all factor interactions.

2.14.2. Relative abundance and connection probability of the striatal compartments—We measured the number of voxels in the matrix-like and striosome-like compartments (all voxels with $P > 0.87$) for each subject, with abundance in each compartment expressed as the percent of all suprathreshold voxels. We also measured the probability of connection at the lowest-amplitude voxel in each subject's compartment-specific seed mask. Each of these comparisons aimed to determine whether striosome-like voxels were significantly less abundant than matrix-less voxels, leading us to treat these comparisons as a family of tests. These comparisons were also utilized to demonstrate the validity of our method independently in each cohort, leading us to perform separate twotailed t-tests in each of our three cohorts and in the combined group of 122 participants (four tests for each approach, relative abundance and connection strength). Therefore, we corrected for multiple comparisons using the method of Bonferroni, with significance threshold set at $0.05/8 = 6.3 \times 10^{-3}$.

2.14.3. N-1 analyses and quantitative whole-hemisphere tractography—For both N-1 and whole-hemisphere experiments, we compared the N voxels within each regional mask that projected to either matrix- or striosome-like targets (paired-samples t-tests). We extracted the voxel counts projecting to the two striatal compartments using anatomic regions in three different approaches (masked by 1. our hand-segmented seed

regions, 2. regions from the Harvard-Oxford atlases, or 3. regions from the Talairach atlas), and at two different thresholds for inclusion (0.87 for N-1, 0.55 for atlas-based extraction). In addition, we compared the number of participants with extreme biases in connectivity ($N_{dominant}$:$N_{nondominant}$) between matrix-favoring and striosome-favoring Harvard-Oxford regions, a measure derived from the data in approach 2. above. Despite these differences in methodology, the underlying similarity of these approaches demanded that we treat these comparisons as a family of t-tests. These tests were non-independent, as mask files from each method partially overlapped those of other methods, regions from the left and right hemisphere were almost always biased towards the same compartment (differing only when some hemispheres were neutral), and prior animal literature demonstrated that many regions covary in their bias towards matrix or striosomes. This precluded our use of Bonferroni correction. Therefore, we utilized the Benjamini-Hochberg procedure (Benjamini and Hochberg, 1995) (N_{tests}=649, false discovery rate=0.05) to correct for multiple comparisons, yielding an adjusted significance threshold of $p < 4.12 \times 10^{-2}$ for all assessments of connectivity by volume. For consistency, we also utilized the Benjamini-Hochberg procedure for the N-1 experiments that extracted data by probability of connection, rather than by volume. In these instances, we included the 10 tests of our N-1 regions (5 regions x 2 hemispheres) and their negative controls (N_{tests}=20, false discovery rate=0.05), which yielded an adjusted significance threshold of $p < 0.025$.

For data extracted at the level of whole hemispheres, plots of matrix-favoring and striosome-favoring volumes appeared heteroscedastic; we confirmed heteroscedasticity with the White test. This was true when considering the two hemispheres separately, or when combined as a whole-brain assessment of connectivity. Therefore, we compared the percentage of matrix-favoring and striosome-favoring extrastriate gray matter (both hemispheres) in each individual using a single two sample *t*-test with unequal variance.

2.14.4. Diffusion metrics—We performed two paired-samples t-tests that compared diffusion values between the striatal compartments, one for mean FA and one for mean MD. The Bonferroni-corrected significance threshold for mean diffusion measures was set at $p < 0.025$.

2.14.5. Regional specificity of striosome connectivity—We quantified the number of striosome-like voxels in each of four areas: rostral caudate, rostral putamen, caudal caudate, and caudal putamen. We had no *a priori* evidence that human striosomes would be organized somatotopically, so we set our expected distribution of voxels proportional to the volume of each subregion. We performed chi squared tests comparing our measured to our expected proportions for each of our N-1 striosomal regions, in each hemisphere (10 comparisons). We therefore set a Bonferroni-corrected significance threshold of $p < 0.005$.

2.14.6. Post-hoc analyses—After testing our primary hypotheses, we elected to perform additional analyses to validate our findings in occipitostriate projections. We performed two *t*-tests comparing connectivity between the striatal region enriched in occipitostriate streamlines and (1) either striosome-favoring or matrix-favoring cortices, and (2) in HOA regions whose connectivity with that same striatal region has been mapped

previously using injected tracers in non-human primates (Saint-Cyr et al., 1990; Weiss et al., 2020). The first *t*-test utilized paired samples comparison, while the second utilized comparisons with unequal variance.

3. Results

Following a review of all English-language studies that utilized injectable tracers to study connectivity to the striatal compartments in animals (Supplemental Table 1), we identified eight cortical gray matter regions in which structural connectivity was most likely to favor one striatal compartment: pregenual anterior cingulate, posterior orbitofrontal, anterior insular cortex, basolateral amygdala, primary sensory, gyrus rectus, supplementary motor area, and primary motor cortex. We summed these regions to generate one matrix-favoring and one striosome-favoring mask. We utilized probabilistic CTT (striatum as seed, these two compartment-selective masks as targets) to assign each striatal voxel a probability of structural connection to either matrix-favoring or striosome-favoring cortices. Voxels were selected from the tails of this probability distribution, 1.5 standard deviation (SD) above/below the mean, to identify striatal voxels whose structural connectivity followed a matrix-like or striosome-like pattern. We utilized these compartment-specific striatal masks, to validate our method and to comprehensively map structural connectivity with each striatal compartment in the human brain. A visual summary of the method can be seen in Supplemental Fig. 1. All reported p-values retained significance following correction for multiple comparisons (Section 2.14).

3.1. Anatomical distribution of matrix-like and striosome-like voxels

Prior histologic studies in animals (Graybiel and Ragsdale, 1978; Goldman-Rakic, 1982; Donoghue and Herkenham, 1986, 20; Desban et al., 1993; Eblen and Graybiel, 1995; Gerfen, 1984; Malach and Graybiel, 1986) and humans (Graybiel and Ragsdale, 1978; Faull et al., 1989; Holt et al., 1997) described rostro-caudal and dorsal-ventral gradients in the predominant locations of each compartment: while striosomes may be found throughout the striatum, they are most frequently found in rostral and ventral sites. Our connectivity-based parcellation method identified a similar pattern: striosome-like voxels preferentially occupy rostral and ventral parts of the striatum (Fig. 1A, B). Within these regional trends, however, striosome placement was unique to each individual (Fig. 1C-G). Four-factor ANOVA, examining the effect of scanner, ethnicity, gender, and striatal compartment on voxel location, identified a significant four-way interaction for both rostral-caudal location ($F(2, 122)=6.23$, $p < 1 \times 10^{-8}$) and dorsal-ventral location ($F(2, 122)=3.98$, $p < 1 \times 10^{-8}$). For both axes, striatal compartment was the only factor with influence on voxel location (rostral-caudal, $F = 29.1$, $p < 1.8 \times 10^{-7}$; dorsal-ventral, $F = 7.62$, $p < 6.3 \times 10^{-3}$). Between-factor interactions generally had little impact on voxel location; for the dorsal-ventral axis only, there was a significant scanner-compartment interaction ($F = 3.73$, $p < 0.012$). Simple main effects analysis of the scanner-compartment interaction showed that there were no significant differences in voxel location when scanned on the Philips Ingenia ($F = 0.12$), but significant differences for cohorts collected on all other scanners ($F = 4.85–36.8$). The Ingenia sub-sample was smaller ($n = 3$) than those for other scanners, potentially limiting the effect in this cohort.

3.2.   Relative abundance of matrix-like and striosome-like voxels

As measured by histology, striosomes comprise approximately 15% of striatal volume (Holt et al., 1997; Desban et al., 1993; Mikula et al., 2009). In our 122 participants, striosome-like voxels made up 15.9% of striatal volume. Supra-threshold voxels (those with $P > 0.87$) were 2.2x more likely to be in the matrix-like than the striosome-like compartment. This was true when we combined Cohorts ($p < 5.1 \times 10^{-16}$), and in separately-measured Cohorts (range of p-values, $1.3 \times 10^{-3} – 8.9 \times 10^{-18}$). In the less-abundant striosome-like compartment, identifying highly-segregated voxels necessitated dipping farther into the probability distribution: the mean value of the lowest-probability voxel in matrix-like masks was 0.954, while for striosome-like voxels it was 0.819 ($p < 1.7 \times 10^{-17}$). This was also true in each Cohort, measured separately (range of p-values, $1.1 \times 10^{-3}–2.6 \times 10^{-13}$).

3.3.   Reproducibility of parcellations

We assessed test-retest reliability of our striatal parcellations in fourteen participants that were scanned twice, with one month between scans. Comparing the location of parcellated voxels between scan1 and scan2, only 9 of 6658 voxels converted between compartments, an error rate of 0.14%. Voxels identified as matrix-like or striosome-like were very unlikely to convert between compartments in a subsequent scan.

3.4.   Comprehensive assessment of structural connectivity with striatal compartments

We selected "bait" regions for our initial striatal parcellation based on prior animal studies and their utility for segregating striatal voxels. While these regions were highly effective as a first-pass assessment, we selected them based on data from other species – these were not optimized for quantifying extra-striate connectivity in humans. Prior tract tracing studies utilized a variety of injected tracers and animal species, a minority of brain regions were investigated with injected tracers, and quantitative comparisons between regions were uncommon. We undertook a comprehensive assessment of striatal compartment connectivity in three steps.

First, we performed whole-hemisphere tractography, with extrastriate regions acting as seeds and the parcellated striatum (equal-volume masks) serving as competitive targets for CTT (Fig. 2). This identified the human brain regions with the largest biases toward one compartment, which was essential to optimizing striatal parcellation for subsequent efforts to quantify structural connectivity. We identified ten regions that had (1) highly segregated connectivity, (2) relative homogeneity in bias across the region, and (3) agreement with animal tract-tracing data. Second, we used these ten regions as seeds for CTT to quantify striatal connectivity in those highly-biased regions (below, "N-1 analyses"). Third, we quantified connectivity in a second round of whole-hemisphere CTT, with connection probability reported according to the regions defined in common neuroanatomic atlases (below, "regions from standard atlases"). Given the similarity of measures in steps 2 and 3, we treated these measures as a family of tests for family-wise error correction (Section 2.14.3).

3.5. Quantitative structural connectivity: N-1 analyses

We used the ten gray matter regions whose connectivity was most-biased towards one striatal compartment (five matrix-favoring, five striosome-favoring) as bait/test regions. We parcellated the striatum using nine of these regions, leaving the tenth region out; rotating the left-out region, we generated 20 distinct "N-1″ striatal parcellations (ten regions, two hemispheres). Using the left-out region as a seed volume for CTT, we assessed the relative strength of structural connectivity with the corresponding (N-1) matrix-like and striosome-like voxels (equal-volume striatal masks). For each hemistriatum, we quantified connectivity through two methods: first, the mean probability of connection between non-zero voxels in the region and each striatal compartment (Fig. 3A); second, the number of voxels in a region with robust connectivity ($P > 0.87$) with each striatal compartment (Fig. 3B). As a negative control, we assessed connectivity between each seed region and non-specific striatal targets (in contrast with the precisely defined matrix-like and striosome-like voxels selected by connectivity).

For all ten regions, two hemispheres, and two methods of quantification (40 total comparisons), structural connectivity was significantly weighted towards either the matrix-like or striosome-like compartment (Fig. 3: p-values ranged from 1.0×10^{-8} to 1.6×10^{-71}; FWE-corrected significance threshold, $p < 4.12 \times 10^{-2}$). When utilizing imprecise striatal masks (negative controls, our 3D checkerboard pattern), structural connectivity had no bias toward either striatal compartment ($p > 0.05$ for all comparisons). In all 40 comparisons, our findings matched those of prior animal histology studies that utilized injectable tract tracers (Supplemental Table 1).

3.6. Quantitative structural connectivity: regions from standard atlases

Many brain regions have never been assessed for striatal compartment selectivity, either because those regions did not align with prior experimental aims or because those regions do not exist in experimental animals. We parcellated the striatal compartments using the ten "N-1″ regions – supplementary motor area, primary motor cortex, primary sensory cortex (Brodmann areas 1–3), the VLc and VPLo thalamic nuclei (combined), the globus pallidus interna, posterior orbitofrontal cortex, basal operculum, anterior insula, basolateral amygdala, and mediodorsal thalamus – and assessed for striatal compartment selectivity in all other brain regions. We comprehensively quantified structural connectivity between the striatal compartments and extrastriate gray matter regions using CTT (Table 1: Harvard-Oxford Atlas (HOA) regions; Supplemental Table 2: Talairach Atlas regions). We utilized a significance threshold (corrected for multiple comparisons, see Section 2.14.3) of $p < 2.5 \times 10^{-2}$ for measures of connection probability and $p < 4.12 \times 10^{-2}$ for volumetric measures. We assessed 102 HOA regions of interest (ROIs); 27 ROIs were matrix-favoring (26%), 57 ROIs were striosome-favoring (56%), and 18 ROIs did not reach our significance threshold (18%). In 6/51 HOA region-pairs, connectivity was significantly biased for only one hemisphere, but connectivity biases were never discordant (even to a non-significant degree) between the two hemispheres. Of the 51 paired regions, only six had no bias in connectivity for both hemispheres: superior temporal gyrus, posterior division; middle temporal gyrus, posterior division; lateral occipital cortex, superior division; cingulate gyrus, posterior division; Heschl's gyrus; planum temporale. Of the structures assessed by

injectable tract tracers that mapped unambiguously to HOA regions (Supplemental Table 1, Table 1), our MRI-based method confirmed the findings of prior histology studies in 13 of 14 regions. Primary visual cortex, which overlaps with both the Intracalcarine and Supracalcarine labels in the Harvard-Oxford Atlas, was reported to be matrix-favoring in animals, and striosome-favoring in our method. Three regions with mixed connectivity in animals were striosome-favoring in this study (frontal pole, cuneal cortex, and lingual gyrus). It should be noted that the relatively large anatomical divisions of the HOA often do not align with the boundaries of striatal compartment selectivity. Some degree of averaging within a region is inevitable, and readers should take these regional observations as a starting point for investigation rather than a categorical assignment.

Talairach regions revealed a similar pattern of biased connectivity, though with smaller differences between categories: 38.1% matrix-favoring, 47.4% striosome-favoring, and 14.5% did not reach our significance threshold (Supplemental Table 2). One notable difference between the Talairach and Harvard-Oxford Atlases is the inclusion of 22 brainstem regions in the former, 91% of which projected preferentially to the matrix. As the Talairach Atlas included many more anatomical subdivisions, this atlas provides a more granular map of striosome/matrix connectivity.

We assessed regional biases in striatal connectivity in two ways: the probability of projecting to the dominant compartment (group mean); and the probability that connectivity in any one subject would be extremely biased (>95% probability of connection to the dominant compartment, expressed as the ratio of the number of participants, $N_{dominant}:N_{nondominant}$). These measures were highly correlated, suggesting that the biases in connectivity were not driven by extreme differences among a minority of subjects (Table 1, Supplemental Table 2). The three HOA regions with greatest bias towards the matrix compartment were: precentral gyrus, juxtapositional lobule, and superior parietal lobule. The three HOA regions with greatest bias towards the striosome compartment were: frontal orbital cortex, intracalcarine cortex, and posterior temporal fusiform cortex. Among HOA regions, right-sided biases were generally more extreme than left hemisphere biases: 32 regions were more biased on the right; only 7 were more biased on the left. Right hemisphere biases were larger in both matrix-favoring and striosome-favoring regions.

We identified both matrix-favoring and striosome-favoring voxels within all tested HOA and Talairach regions, even when mean connectivity strongly favored one striatal compartment. These regional assessments are averages, and large ROIs inevitably include a combination of matrix-favoring and striosome-favoring voxels. A good example of this complexity can be seen in the left HOA Insular Cortex (Fig. 4). Prior tract tracing studies in macaque (Eblen and Graybiel, 1995) and cat (Ragsdale and Graybiel, 1990) demonstrated that the rostral insula selectively projects to striosomes. Segmentations that isolate the rostral two gyri from the posterior insula reveal strong biases in connectivity that were not evident at the whole-region level: the rostral insula favored striosome-like voxels ($P_{striosome}=73.6\%$, $p < 1.90 \times 10^{-18}$), while caudal insula favored matrix-like voxels ($P_{Matrix}=62.7\%$, $p < 7.49 \times 10^{-5}$).

3.7. Distinct structural connectivity for each striatal compartment

We set striosome-like and matrix-like striatal masks as seeds for probabilistic tractography (equal-volume seeds, restricted to the ipsilateral hemisphere, otherwise unbounded). The two compartments produced streamline volumes that were largely segregated; the Dice similarity coefficients for left and right hemispheres were $12.0 \pm 0.8\%$ and $13.9 \pm 0.8\%$, respectively. Streamlines contacting matrix-like seeds reached more voxels than those contacting striosome-like seeds (15.7% larger volume of distribution; left, 27,335 vs. 22,846 mm^3, $p < 3.84 \times 10^{-6}$; right, 26,223 vs. 22,312 mm^3, $p < 1.19 \times 10^{-4}$). This finding mirrored our observation in whole-hemisphere CTT (Section 3.6, using extrastriate voxels as seeds and parcellated striatal compartments as targets): voxels that project to matrix-like targets make up a larger share of the extrastriate brain (combined hemispheres, 28.9% to matrix-like, 26.8% to striosome-like targets, $p < 0.0265$). This finding replicates the matrix-dominated cortical connectivity demonstrated by Smith et al. in mice (Smith et al., 2016). Peak streamline count did not differ between tractography seeded by matrix-like and striosome-like voxels. However, when streamlines were quantified at the level of seed voxels, rather than from distributed tractograms, striosome-like voxels generated 16.1% more cortex-contacting streamlines than an equal number of matrix-like voxels (mean streamlines/hemisphere, 89,131 vs. 76,772, $p < 2.49 \times 10^{-6}$). With greater numbers of streamlines contacting a smaller volume of distribution, we estimate that the streamline density of tracts reaching striosome-like voxels is >1/3 higher than for tracts reaching matrix-like voxels.

Careful readers may have noted that matrix-favoring connectivity dominated when quantified by individual voxels (tractography seeded by striatal or whole-hemisphere extrastriate voxels), but more regions were striosome-favoring than matrix-favoring. By design, region-of-interest methods average results across a volume, potentially diluting voxels that are supra-threshold but outnumbered. We quantified the matrix-favoring voxels within striosome-favoring HOA regions, and the striosome-favoring voxels within matrix-favoring HOA regions. Striosome-favoring regions incorporated more matrix-favoring voxels than the obverse (35.0% matrix-within-striosome vs. 25.1% striosome within-matrix, $p < 0.0174$). Region-of-interest based extraction also incorporated voxels with no data – the majority of extrastriate gray matter voxels did not generate streamlines that reached the small fraction of voxels that we defined as striatal targets. These "empty" voxels were more prevalent in striosome-favoring regions than in matrix-favoring regions (left, 50.3% greater, $p < 5.37 \times 10^{-70}$; right, 62.8% greater, $p < 2.06 \times 10^{-62}$). Thus, while more regions were striosome-favoring, these regions were significantly more likely to include "empty" or conflicting voxels. Matrix-favoring voxels were clustered at higher density in matrix-favoring regions and were distributed more broadly within the extrastriate gray matter.

3.8. Regional specificity of striosome connectivity

Prior tract tracing studies demonstrated that cortical regions with biased striatal connectivity do not project to all parts or matrix or striosome; rather, projections are organized somatotopically (Donoghue and Herkenham, 1986, 20; Eblen and Graybiel, 1995; Malach and Graybiel, 1986; Berendse et al., 1988). Similarly, we found that striosome-like voxels

whose connectivity was dominated by one N-1 region are found in distinct zones (Fig. 5). We quantified somatotopic organization by rostro-caudal position and by location within the caudate or putamen. These zones were highly similar between hemispheres for three striosome-favoring regions: mediodorsal thalamus, dense cluster in rostral caudate (100% segregation: left, $p < 3.56 \times 10^{-48}$; right, $p < 1.62 \times 10^{-39}$); basal operculum, dense cluster in rostral putamen (100% segregation: left, $p < 8.28 \times 10^{-60}$; right, $p < 4.73 \times 10^{-53}$); rostral insula, dispersed with two-thirds of voxels in posterior putamen and one-third divided between rostral caudate and rostral putamen (left, $p < 1.25 \times 10^{-10}$; right, $p < 3.96 \times 10^{-27}$). In both hemispheres, basolateral amygdala demonstrated a dispersed pattern that favored the putamen (nine-tenths of voxels: left, $p < 6.99 \times 10^{-50}$; right, $p < 3.23 \times 10^{-9}$), but the hemispheres differed in their rostro-caudal distribution of voxels (left, 100% caudal; right, 34% caudal). Voxels strongly-influenced by the posterior orbitofrontal were dispersed widely in both caudate and putamen, rostral and caudal, without a clear predilection for an identifiable zone (left, $p < 2.90 \times 10^{-44}$; right, $p < 8.14 \times 10^{-7}$). Overlap between zones, indicating co-dominance of two striosome-favoring regions, occurred in 1.5% of voxels; most overlapping voxels (87%) were attributable to the posterior orbitofrontal cortex, our least somatotopically-segregated region.

Regional specificity was also evident within extra-striate areas whose projections were biased towards striosomes. Connectivity between the mediodorsal thalamus and ipsilateral striosome-like voxels has not been mapped using injected tract tracers, to the best of our knowledge (Supplemental Table 1). However, striatal zones are the target of convergent projections from functionally related cortical and thalamic areas (as demonstrated for motor-related projections to the striatum (McFarland and Haber, 2000; Takada et al., 2001)). We reasoned that the mediodorsal thalamus – whose connectivity with cortical regions that project selectively to striosomes is well-established (Phillips et al., 2019; Goldman-Rakic and Porrino, 1985; Vogt et al., 1987; van Vulpen and Verwer, 1989; O'Muircheartaigh et al., 2015) – might be the third limb in such a cortico-striatal-thalamic loop. We aimed to bolster this hypothesis by confirming that mediodorsal voxels with strong striosome-favoring connectivity colocalize with corticothalamic projections from cortical areas that also selectively project to striosomes. We confirmed that striosome-favoring connectivity is strongest in the dorsolateral and anterior portions of the mediodorsal thalamus (aligning with the enrichment of prefrontal cortex projections to the parvocellular portion of the mediodorsal thalamus (Phillips et al., 2019; Goldman-Rakic and Porrino, 1985)), and follows a decreasing rostral-caudal gradient within the mediodorsal thalamus (Supplemental Fig. 2).

3.9. Diffusion properties of matrix-like and striosome-like voxels

Mean fractional anisotropy (FA) was higher in matrix-like than in striosome-like voxels (equal-volume masks, Fig. 6A, combined hemispheres: matrix (0.229) vs. striosome (0.200), $p < 3.41 \times 10^{-9}$). Matrix-like and striosome-like voxels did not differ in mean diffusivity (MD; matrix vs. striosome, 9.70×10^{-4} vs. 9.28×10^{-4}; $p < 0.0835$).

We considered the possibility that these differing mean FA values might bias connectivity, independent of matrix/striosome segregation; that is, that our connectivity-based striatal

parcellations might have been compromised by the differing FA values in matrix-like and striosome-like voxels. Therefore, we performed a second striatal parcellation as a negative control, using mean FA value to define striatal masks instead of matrix-like and striosome-like connectivity. These FA-defined masks matched our matrix/striosome parcellations for size and mean FA. Using four extrastriate regions as seeds, suggested by both animal tract tracing studies in animals and our own results (Fig. 2, Supplemental Table 1) to be among the most highly-segregating cortical regions (primary motor and sensory to matrix, basal operculum and posterior orbitofrontal to striosome), and these FA-defined, equal-volume striatal masks as classification targets, we tested whether differences in FA drove the striosome-like and matrix-like patterns of connectivity. Both striosome-favoring and matrix-favoring cortices displayed a marked preference for the higher FA striatal target (Fig. 6B, ratio of high-to-low connectivity: primary motor, 4.5-fold preference for the higher FA voxels, $p < 1.20 \times 10^{-144}$; primary sensory, 4.3-fold, $p < 7.78 \times 10^{-131}$; basal operculum, 2.5-fold, $p < 3.10 \times 10^{-55}$; posterior orbitofrontal, 3.1-fold, $p < 8.39 \times 10^{-55}$). Rather than recapitulating the striosome-favoring projection pattern of the basal opercular and posterior orbitofrontal cortices, FA-based parcellation yielded the opposite pattern, more similar to matrix-favoring regions. Similarly, matrix-favoring regions (primary motor and primary sensory) became less specific when utilizing FA-selected voxels as targets. Therefore, we conclude that differing FA values in matrix-like and striosome-like voxels were not the drivers of segregated patterns of striatal connectivity.

3.10. Occipitostriate structural connectivity

Since our assessment of striatal compartment connectivity differed from that in rodents (occipital cortex is striosome-favoring in humans, matrix-favoring in rats), we sought a deeper understanding of occipitostriate connectivity that might explain this disparity. We investigated structural connectivity between the whole striatum and two occipital regions with strong biases in striatal compartment connectivity: Brodmann areas 17 and 18 (BA17, BA18). The core projections for BA17 and BA18 each localized to the ventral-posterior putamen (VPP, Fig. 7); the volume of overlap between the core projections of BA17-18 to VPP was 84% and 87% for the left and right hemispheres, respectively. This result is highly similar to prior efforts to systematically assess corticostriate connectivity using probabilistic tractography (Tziortzi et al., 2014), which identified a putaminal zone enriched in occipitostriate projections that overlaps the VPP (Tziortzi et al., 2014, Fig. 1B). We next assessed connectivity between the VPP and striosome-favoring and matrix-favoring regions. This provided an independent, though indirect, check on our previous finding that the visual cortices project more to striosome-like than to matrix-like voxels. We hypothesized that if BA17-18 projections to striatum are relatively specific for VPP, and if our prior finding that BA17-18 projections favored the striosome-like compartment is accurate, then corticostriate streamlines reaching VPP from striosome-favoring cortices should outnumber those originating in matrix-favoring cortices.

We found that voxels in striosome-favoring cortices generated 8.9-fold more streamlines that contacted VPP than voxels in matrix-favoring cortices ($p < 6.54 \times 10^{-27}$). We identified this striosome-favoring pattern of VPP connectivity in 89% of the 244 tested hemispheres. It must be noted that we identified this pattern of biased connectivity without utilizing the

striatal parcellation method described for all other parts of this report. Finally, we quantified the per-voxel connectivity with VPP for each HOA cortical region. While BA17-18 streamlines were highly specific for VPP, the VPP also received streamlines from many other cortical regions; the three regions with the highest connectivity (average streamlines per voxel) with VPP were planum polare, temporal pole, and frontal orbital cortex. We identified one cortical area that aligned neatly with HOA regions whose connectivity with the VPP was previously mapped by injected tracers in primates (Saint-Cyr et al., 1990), the middle temporal gyrus (MTG). As in the macaque, projections from the human MTG were highly enriched in the VPP: 73.5% of MTG voxels seeded streamlines that reached the VPP, and the average MTG voxel seeded 263 streamlines. In contrast, two regions for which retrograde tracer injections identified high connectivity with anterior and middle, but not posterior putamen (paracingulate and middle frontal gyrus) (Weiss et al., 2020) had minimal connectivity with the human VPP. In these gyri only 22.6% of voxels seeded streamlines that reached the VPP, generating 8.6 streamlines/voxel, a 31-fold reduction in mean streamlines/ voxel relative to the MTG ($p < 4.0 \times 10^{-31}$). Intracalcarine cortex (the closest HOA equivalent of Talairach BA17) had the 15th highest mean connectivity with VPP (of 48 HOA regions). However, relative to the planum polare (the HOA region with the strongest tractographic connectivity with VPP), intracalcarine cortex had 8.2-fold higher bias towards the striosome-like compartment (Table 1B) despite having 6.3-fold lower streamlines per voxel. This underscores the fact that the magnitude of striatal connectivity, and bias of connectivity toward one striatal compartment, are independent factors.

4. Discussion

For four decades, animal studies have demonstrated that the matrix and striosome compartments are embryologically, anatomically, histochemically, hodologically and functionally distinct. However, the dependence on immunohistochemical techniques or genetic manipulation to distinguish the striatal compartments has substantially impeded the characterization of matrix and striosomes in humans. Since nearly all parts of the human diencephalon and telencephalon have afferent or efferent connections with the striatum, our scant knowledge of matrix- and striosome-specific biology is a major limitation in understanding the ways that the striatum refines and regulates cortical and thalamic projections. Such characterization is essential to understanding how these segregated tissue compartments function in human health and disease.

We parcellated the human striatum based solely on patterns of structural connectivity. In so doing, we identified voxels that independently replicated properties of matrix and striosomes previously identified in animals: a spatial gradient, with striosomes concentrated in rostroventral sites; somatotopic organization of compartment-specific projections; highly segregated patterns of connectivity that matched tract tracing studies for 93% of previously-mapped regions. We also identified regions with compartment-favoring connectivity that had never been mapped, in any species. Utilizing striatal voxels that are imprecisely placed, or selected based on FA rather than on biased structural connectivity, abolishes these effects. Despite the strength of these findings, we must emphasize that our method identified voxels that share features with the striatal compartments – hence are matrix-like and striosome-like – but our inferential process does not directly identify matrix or striosomes. Confirmation of

this method with combined immunohistochemical and diffusion MRI characterization in the same (postmortem) brain will be necessary to substantiate these findings.

We identified a strong bias in connectivity between visual cortex (all subregions) and striosome-like voxels. Among the 102 HOA regions, those corresponding to visual cortex were the sole regions that disagreed with prior data from animal tract tracing studies. It is possible that systematic distortions of DTI signal in occipital regions alters corticostriate connectivity. However, no such distortion is evident on direct visualization, and it is not clear why a theoretical distortion would bias connectivity toward striosomes. A close reading of the two studies that assessed visual cortex-striate connectivity in rat suggests that primary visual cortex may display a mixed pattern of projection rather than projecting exclusively to matrix: Donoghue and Herkenham found that visual cortex projections "mainly occupy the matrix" (Donoghue and Herkenham, 1986), and Lopez-Figueroa et al. (1995) noted that visual cortex projections overlapped striatal zones with absent staining for either calbindin or opiate ligands, markers of matrix and striosomes, respectively. This mixed pattern of connectivity would align with that of visual association cortex, the only other part of visual cortex assessed in prior compartment-specific tract tracing studies.

Another potential explanation for our findings in the visual cortices is mis-tracking of diffusion streamlines. We compared human tractographic and animal tract tracing data in 14 regions – a fiber tracking error in 1 of 14 regions would not be surprising given the limitations in reconstructing white matter pathways when using diffusion MRI data in isolation (Schilling et al., 2019). Therefore, we sought to assess the validity of this finding using corticostriate tract tracing studies in non-human primates. Saint-Cyr et al. utilized anterograde and retrograde tracers in macaques to map projections from non-primary visual cortices to the striatum (Saint-Cyr et al., 1990). They localized visual cortical projections in macaque (their Fig. 19) to a ventral-posterior site that overlaps precisely with the striatal region we identified (VPP, Fig. 7) as the predominant contact for streamlines between the striatum and Brodmann areas 17 and 18. Likewise, Campos-Ortega identified a small bundle of fibers that projected from Brodmann areas 17, 18, and 19 to the "caudal end of the putamen" in the prosimian *Galago crassicaudatus* (later reclassified as *Otolemur crassicaudatus*) (Campos-Ortega, 1968). A similar projection from the dorsomedial visual area (a subdivision of Brodmann area 19) to the caudal putamen was identified in the owl monkey (*Aotus trivirgatus*) (Norden et al., 1978). In macaque, visual areas apart from Brodmann areas 17-19 also project specifically to the posterior putamen, including Area V4 (Gattass et al., 2014), the superior temporal sulcus (Maioli et al., 1983), middle temporal (MT, or V5) (Ungerleider et al., 1984) inferior temporal (TE and TEO) (Webster et al., 1993), lateral inferotemporal (Yeterian and Pandya, 1995), and the dorsolateral-middle temporal crescent areas (DL-MTC) (Weller et al., 2002). While not all of these articles illustrated their putaminal findings, figures that demonstrated the putaminal zone targeted by these non-primary visual areas had a high degree of overlap with the VPP (Gattass et al., 2014; Webster et al., 1993; Yeterian and Pandya, 1995). In an important counterfactual, ventromedial visual cortex (Brodmann Area 19, or area V2v) projects to the extreme posterior putamen, but to a zone dorsal to the VPP (Yeterian and Pandya, 1995). It should be noted that many of these non-primary visual areas project to the caudate tail. We found that this thin, tubular structure frequently suffers from poor registration and volume averaging

with the white matter surrounding it. Therefore, we did not include the caudate tail in this analysis. We hope that future studies assessing the connectivity between visual cortices and the striatal compartments will overcome this technical challenge.

Projections from visual cortices to the striatum are not unique to primates. In the rabbit, complete lesion of Brodmann area 18 (and the caudal portions of Brodmann area 17) produced degenerating fibers that filled the "whole width of the posterior quarter of the putamen" (Carman et al., 1963). In the cat, lesion of the primary visual cortex led to degeneration of a small band in the superior caudate (Webster, 1965) – in contrast with the caudal putamen – underscoring that while species may differ in the exact location of striate targets, such occipitostriate projections are common across multiple mammalian species. Given the fact that visual cortical projections to the posterior putamen exist in multiple primate and non-primate species, that our tractographic method recapitulated the striatal zone identified through injected tract tracing experiments as the specific target of projections from visual cortical areas (the VPP), and that our tractographic quantification of connectivity with VPP agrees with prior tract-tracing experiments in macaque (Section 3.10), it appears unlikely that our occipitostriate findings are purely the result of fiber mis-tracking.

While convergence of our tractographic findings and prior histologic assessments is reassuring, it is important to acknowledge that substantial uncertainty persists regarding the projections from primary and secondary visual cortices to the striatum. While Saint-Cyr et al. mapped multiple parts of the striatum with multiple visual cortical areas, they did not map the whole of the primary or secondary visual cortices, and their striatal injections of retrograde tracers fell anterior to the putaminal area corresponding to the VPP (their Fig. 10). Similarly, in a modern effort to map corticostriate projections, Weiss et al. utilized an AAV2 vector with enhanced retrograde transport in macaque.[82] They found that projections from occipital cortex to the striatum were effectively non-existent. However, their AAV2 vector did not infect the posterior putamen or the tail of the caudate (their Fig. 2a), sites that were demonstrated to be targets of occipitostriate projections in other primate experiments (Saint-Cyr et al., 1990). We identified only two primate studies that utilized anterograde tracers (tritiated amino acids) to map projections from BA17–18 that commented on striatal connectivity (Graham et al., 1979; Ungerleider et al., 2014). Graham et al. identified no "substantial projection" from BA17 to the caudate or putamen, while projections from BA18 were "very sparse." Ungerleider et al. injected a broad swath of sites in BA18 and found no projections to the caudate or putamen.

At least two possible explanations exist for this discrepancy between connectivity assessed by injected tracers and by diffusion tractography. First, tractography samples all voxels within a seed volume, while injected tracers cannot reach all portions of a target region – even when investigators expend substantial effort to map a region (Ungerleider et al., 2014). The portions of BA17 and 18 that originate projections to the VPP may simply be distinct from those injected in the limited number of primates reported to date. Second, CTT quantifies differential connectivity, not absolute connectivity. The projections from BA17 and 18 may be "very sparse," as Graham et al. found, but highly biased toward one target – in this case, toward striosome-like voxels. Indeed, we found that streamlines from intracalcarine cortex (the Harvard-Oxford atlas region corresponding most closely

to BA17) were highly specific for the VPP, but had 6.3-fold lower streamlines per voxel than high-connectivity cortical areas. Both Graham et al. and Ungerleider et al. identified projections using autoradiography, a method that does not incorporate signal amplification. Detecting low-abundance projections with autoradiography requires that one optimize signal for low-intensity regions, overexposing high-intensity regions – often the regions that are the primary focus of investigation. Therefore, unless an autoradiography study has been optimized to detect low-abundance projections in the striatum, lack of signal is not proof of a lack of connectivity. While future experiments are necessary to investigate this discrepancy for primary visual cortices, the ability of our MRI method to replicate all other previously reported regional biases, and the fact that the occipitostriate circuit we identified parallels tract tracing studies in multiple primate and non-primate species, underscores the reliability of our parcellation technique.

One limitation of our MRI-based method is the relatively-large voxel size (2 mm isotropic) commonly utilized for DTI scans. At this resolution even perfectly-centered striosomes will be averaged with some volume of surrounding matrix, diluting between-compartment differences. Indeed, this is potentially why striosome-favoring regions included many matrix-favoring voxels. Despite this limitation, our ability to identify striosome-like voxels with highly segregated patterns of connectivity was robust. Likewise, similarly-sized voxels have been successfully utilized to derive >100 corticostriate functional and structural covariance networks (Ogawa et al., 2018; Liu et al., 2020). One caveat to these results is that striosome-like voxels in some individuals are found in clusters larger than one might predict – in some cases 4–6 contiguous voxels in the coronal plane (Fig. 1F), where one would expect smaller clusters if a striosome were divided between adjacent voxels. Whether this is a partial volume effect, single striosomes spreading across contiguous voxels as they branch in three dimensions, the presence of disconnected "exo-patch" neurons within surrounding matrix (Smith et al., 2016), or error in our parcellation technique, is insoluble at this resolution. We propose that sub-millimeter resolution DTI, now possible with 3T scans of clinically-feasible duration (Ramos-Llorden et al., 2020), may yield substantial gains in our ability to precisely delineate striosomes. Likewise, tractography cannot make fine distinctions at the level of single axons or synapses, making it difficult for our probabilistic method to parcellate voxels from regions that generate dual-synaptic connections in both compartments (Smith et al., 2016; Kincaid and Wilson, 1996), and cortical regions in which adjacent cortical layers innervate different compartments (Gerfen, 1989; Kincaid and Wilson, 1996; Levesque and Parent, 1998). Indeed, this is a potential explanation for why many cortical voxels had a neutral compartment bias.

How might characterization of human striatal diseases at the compartment level help improve patient outcomes? Identifying distinct compartment-specific susceptibilities may suggest differing neuroprotection strategies for matrix-specific and striosome-specific diseases. Detecting tissue injury in the compartments, before it is evident at the whole-striatum level, may allow earlier initiation of neuroprotective therapies. In disorders with progressive loss of MSNs, it is unlikely that injury is uniform across a compartment – understanding which striosomes, or which parts of the matrix, are abnormal is key to understanding specific pathophysiologies. The evolution of symptoms in neurodegenerative diseases (e.g., from one type of movement disorder to another, as seen in Huntington disease

(Morton et al., 1993) and XDP (Goto et al., 2005)) has suggested that injury may evolve from compartment-specific to pan-striatal (Crittenden and Graybiel, 2011). Our method can test these hypotheses *in vivo,* potentially suggesting pathophysiologic mechanisms that are obscured when studies are limited to post-mortem histology.

Diseases with overt pathology are understandably an initiation-point for understanding striatal diseases, but most disorders with hypothesized compartment-specific dysfunction (Crittenden and Graybiel, 2011) have no gross anatomical correlate. Our technique can identify compartment-specific seeds for other imaging techniques, such as fMRI or PET, that can be used to elucidate functional networks. Though beyond the scope of this report, we speculate that compartment-informed functional networks may distinguish between disease subtypes more accurately than networks derived from whole-striatum approaches. Indeed, the derivation of corticostriate networks through boundary mapping of functional connectivity has already driven hypotheses that striosomes may be targets of specific functional networks (Ogawa et al., 2018). Connectivity-based striatal parcellations are highly stable between MRIs performed one month apart, suggesting that this method may be useful in longitudinal studies of human disease or development. Indeed, neurosurgical interventions to treat movement or mood disorders, including deep brain stimulation, may be more effective if intranuclear targets (e.g., what point within the globus pallidus) are selected based on more precise knowledge of compartment-specific somatotopy. *In vivo* investigation of the striatal compartments is indispensable for understanding both striatal diseases and a range of cognitive and substance-use disorders (Crittenden and Graybiel, 2011).

Compartment-specific and somatotopically-selective functions are likely relevant to normal learning and reward as well. As has been demonstrated with motor performance learning (Nadel et al., 2020; Lawhorn et al., 2009), stimulus-response learning (Jenrette et al., 2019), and value-influenced decision-making (Friedman et al., 2015) paradigms in rodents, directly targeting striosomes impedes the acquisition of tested behaviors, an impairment not seen in matrix-specific stimulation. In self-stimulation paradigms, rats acquired and maintained lever-pressing responses significantly more when electrodes contacted striosomes than when they contacted matrix (White and Hiroi, 1998). Similarly, repeated cocaine exposure in non-human primates (Saka et al., 2004) and in rats (Canales and Graybiel, 2000) sensitizes striosome neurons more than matrix neurons; increased striosome-specific expression of immediate-early genes is highly correlated with increased cocaine- or methamphetamine-induced motor stereotypies (Saka et al., 2004; Canales and Graybiel, 2000). Striosomes are more susceptible to selective activation by Graybiel et al. (1990) and toxicity from methamphetamine (Granado et al., 2010) and MDMA (Granado et al., 2008), potentially due to their higher intrinsic excitability (McGregor et al., 2019). These observations suggest that striosomal abnormalities might underlie the range of susceptibilities to addiction. Determining whether human striosomal MSNs are susceptible to substance-induced excitotoxicity, and whether striosomal connectivity is abnormal in addiction, are potential applications of connectivity-based parcellation. In adolescents, frequent use of addictive substances, and an increased range of substances used, correlates with increased functional connectivity between hippocampus and the striosome-enriched ventral striatum (Huntley et al., 2020). We found that hippocampal structural connectivity is significantly biased towards striosome-like voxels (Table 1B), an anatomical relationship not reported

previously. Whether hippocampo-striosomal structural connectivity drives increased reward, or whether striosomes mediate reward-sensitive memory formation, remains to be seen.

5. Conclusions

Striatal parcellation based on probabilistic structural connectivity is an accessible and reliable method for distinguishing the matrix-like and striosome-like compartments in living humans. Our approach is modular, allowing researchers to define their own bait/test regions and adjust stringency across a wide range of probability distributions. Segmentation of the striatal compartments may be its own end, for fundamental neuroanatomic questions, or may provide the seeds for investigations of striatal functions and human striatal diseases using other imaging methods. Given the central role of the striatum in regulating cortical and thalamic activity, understanding the functions of the matrix and striosome compartments is an essential next step in human neuroscience.

Supplementary Material

Refer to Web version on PubMed Central for supplementary material.

References

Kawaguchi Y, Wilson CJ, Emson PC, 1989. Intracellular recording of identified neostriatal patch and matrix spiny cells in a slice preparation preserving cortical inputs. J. Neurophysiol 62, 1052–1068. [PubMed: 2585039]

Smith JB, 2016. Genetic-based dissection unveils the inputs and outputs of striatal patch and matrix compartments. Neuron 91, 1069–1084. [PubMed: 27568516]

McGregor MM, 2019. Functionally distinct connectivity of developmentally targeted striosome neurons. Cell Rep. 29, 1419–1428 .e1415. [PubMed: 31693884]

Crittenden JR, Graybiel AM, 2011. Basal Ganglia disorders associated with imbalances in the striatal striosome and matrix compartments. Front. Neuroanat 5, 59. [PubMed: 21941467]

Mandemakers W, Snellinx A, O'Neill MJ, de Strooper B, 2012. LRRK2 expression is enriched in the striosomal compartment of mouse striatum. Neurobiol. Dis 48, 582–593. [PubMed: 22850484]

West AB, 2014. Differential LRRK2 expression in the cortex, striatum, and substantia nigra in transgenic and nontransgenic rodents. J. Comp. Neurol 522, 2465–2480. [PubMed: 24633735]

Morigaki R, Goto S, 2015. Postsynaptic density protein 95 in the striosome and matrix compartments of the human neostriatum. Front. Neuroanat 9, 154. [PubMed: 26648848]

Graybiel AM, Hickey TL, 1982. Chemospecificity of ontogenetic units in the striatum: demonstration by combining [3H]thymidine neuronography and histochemical staining. Proc. Natl. Acad. Sci. U. S. A 79, 198–202. [PubMed: 6172791]

van der Kooy D, Fishell G, 1987. Neuronal birthdate underlies the development of striatal compartments. Brain Res. 401, 155–161. [PubMed: 3028569]

Feekes JA, Cassell MD, 2006. The vascular supply of the functional compartments of the human striatum. Brain 129, 2189–2201. [PubMed: 16815876]

Joel D, Niv Y, Ruppin E, 2002. Actor-critic models of the basal ganglia: new anatomical and computational perspectives. Neural Netw. 15, 535–547. [PubMed: 12371510]

White NM, Hiroi N, 1998. Preferential localization of self-stimulation sites in striosomes/patches in the rat striatum. Proc. Natl. Acad. Sci. U. S. A 95, 6486–6491. [PubMed: 9600993]

Salinas AG, Davis MI, Lovinger DM, Mateo Y, 2016. Dopamine dynamics and cocaine sensitivity differ between striosome and matrix compartments of the striatum. Neuropharmacology 108, 275–283. [PubMed: 27036891]

Stephenson-Jones M, Kardamakis AA, Robertson B, Grillner S, 2013. Independent circuits in the basal ganglia for the evaluation and selection of actions. Proc. Natl. Acad. Sci. U. S. A 110, E3670–E3679. [PubMed: 24003130]

Graybiel AM, Ragsdale CW, 1978. Histochemically distinct compartments in the striatum of human, monkeys, and cat demonstrated by acetylthiocholinesterase staining. Proc. Natl. Acad. Sci. U. S. A 75, 5723–5726. [PubMed: 103101]

Faull RL, Dragunow M, Villiger JW, 1989. The distribution of neurotensin receptors and acetylcholinesterase in the human caudate nucleus: evidence for the existence of a third neurochemical compartment. Brain Res. 488, 381–386. [PubMed: 2545305]

Holt DJ, Graybiel AM, Saper CB, 1997. Neurochemical architecture of the human striatum. J. Comp. Neurol 384, 1–25. [PubMed: 9214537]

Goldman-Rakic PS, 1982. Cytoarchitectonic heterogeneity of the primate neostriatum: subdivision into Island and Matrix cellular compartments. J. Comp. Neurol 205, 398–413. [PubMed: 7096628]

Donoghue JP, Herkenham M, 1986. Neostriatal projections from individual cortical fields conform to histochemically distinct striatal compartments in the rat. Brain Res. 365, 397–403. [PubMed: 3004664]

Ragsdale CW, Graybiel AM, 1990. A simple ordering of neocortical areas established by the compartmental organization of their striatal projections. Proc. Natl. Acad. Sci. U. S. A 87, 6196–6199. [PubMed: 1696719]

Desban M, Kemel ML, Glowinski J, Gauchy C, 1993. Spatial organization of patch and matrix compartments in the rat striatum. Neuroscience 57, 661–671. [PubMed: 8309529]

Eblen F, Graybiel AM, 1995. Highly restricted origin of prefrontal cortical inputs to striosomes in the macaque monkey. J. Neurosci 15, 5999–6013. [PubMed: 7666184]

Tippett LJ, 2007. Striosomes and mood dysfunction in Huntington's disease. Brain 130, 206–221. [PubMed: 17040921]

Sprengelmeyer R, 2014. The neuroanatomy of subthreshold depressive symptoms in Huntington's disease: a combined diffusion tensor imaging (DTI) and voxel-based morphometry (VBM) study. Psychol. Med 44, 1867–1878. [PubMed: 24093462]

De Paepe AE, 2019. White matter cortico-striatal tracts predict apathy subtypes in Huntington's disease. Neuroimage Clin. 24, 101965. [PubMed: 31401404]

Blood AJ, 2017. Increased insula-putamen connectivity in X-linked dystonia-parkinsonism. NeuroImage Clin..

Segawa M, Nomura Y, Hayashi M, 2013. Dopa-responsive dystonia is caused by particular impairment of nigrostriatal dopamine neurons different from those involved in Parkinson disease: evidence observed in studies on Segawa disease. Neuropediatrics 44, 61–66. [PubMed: 23468278]

Sato K, 2008. Differential involvement of striosome and matrix dopamine systems in a transgenic model of dopa-responsive dystonia. Proc. Natl. Acad. Sci. U. S. A 105, 12551–12556. [PubMed: 18713855]

Crittenden JR, 2017. Striatal cholinergic interneurons modulate spike-timing in striosomes and matrix by an amphetamine-sensitive mechanism. Front. Neuroanat 11 20. [PubMed: 28377698]

Jenrette TA, Logue JB, Horner KA, 2019. Lesions of the patch compartment of dorsolateral striatum disrupt stimulus-response learning. Neuroscience 415, 161–172. [PubMed: 31356898]

Nadel JA, Pawelko SS, Copes-Finke D, Neidhart M, Howard CD, 2020. Lesion of striatal patches disrupts habitual behaviors and increases behavioral variability. PLoS One 15, e0224715. [PubMed: 31914121]

Mikula S, Parrish SK, Trimmer JS, Jones EG, 2009. Complete 3D visualization of primate striosomes by KChIP1 immunostaining. J. Comp. Neurol 514, 507–517. [PubMed: 19350670]

Lusebrink F, Sciarra A, Mattern H, Yakupov R, Speck O, 2017. T1-weighted *in vivo* human whole brain MRI dataset with an ultrahigh isotropic resolution of 250 mum. Sci. Data 4, 170032. [PubMed: 28291265]

Gerfen CR, 1984. The neostriatal mosaic: compartmentalization of corticostriatal input and striatonigral output systems. Nature 311, 461–464. [PubMed: 6207434]

Malach R, Graybiel AM, 1986. Mosaic architecture of the somatic sensory-recipient sector of the cat's striatum. J. Neurosci 6, 3436–3458. [PubMed: 3794782]

Berendse HW, Voorn P, te Kortschot A, Groenewegen HJ, 1988. Nuclear origin of thalamic afferents of the ventral striatum determines their relation to patch/matrix configurations in enkephalin-immunoreactivity in the rat. J. Chem. Neuroanat 1, 3–10. [PubMed: 3077313]

Desban M, Gauchy C, Kemel ML, Besson MJ, Glowinski J, 1989. Three-dimensional organization of the striosomal compartment and patchy distribution of striatonigral projections in the matrix of the cat caudate nucleus. Neuroscience 29, 551–566. [PubMed: 2739901]

Gerfen CR, 1989. The neostriatal mosaic: striatal patch-matrix organization is related to cortical lamination. Science 246, 385–388. [PubMed: 2799392]

Jimenez-Castellanos J, Graybiel AM, 1989. Compartmental origins of striatal efferent projections in the cat. Neuroscience 32, 297–321. [PubMed: 2479881]

Langer LF, Graybiel AM, 1989. Distinct nigrostriatal projection systems innervate striosomes and matrix in the primate striatum. Brain Res. 498, 344–350. [PubMed: 2477114]

Gimenez-Amaya JM, Graybiel AM, 1990. Compartmental origins of the striatopallidal projection in the primate. Neuroscience 34, 111–126. [PubMed: 1691462]

Ragsdale CW, Graybiel AM, 1991. Compartmental organization of the thalamostriatal connection in the cat. J. Comp. Neurol 311, 134–167. [PubMed: 1719043]

Sadikot AF, Parent A, Smith Y, Bolam JP, 1992. Efferent connections of the centromedian and parafascicular thalamic nuclei in the squirrel monkey: a light and electron microscopic study of the thalamostriatal projection in relation to striatal heterogeneity. J. Comp. Neurol 320, 228–242. [PubMed: 1619051]

Parthasarathy HB, Schall JD, Graybiel AM, 1992. Distributed but convergent ordering of corticostriatal projections: analysis of the frontal eye field and the supplementary eye field in the macaque monkey. J. Neurosci 12, 4468–4488. [PubMed: 1279139]

Ebrahimi A, Pochet R, Roger M, 1992. Topographical organization of the projections from physiologically identified areas of the motor cortex to the striatum in the rat. Neurosci. Res 14, 39–60. [PubMed: 1380687]

Rajakumar N, Elisevich K, Flumerfelt BA, 1993. Compartmental origin of the stria-to-entopeduncular projection in the rat. J. Comp. Neurol 331, 286–296. [PubMed: 8509503]

Flaherty AW, Graybiel AM, 1993. Two input systems for body representations in the primate striatal matrix: experimental evidence in the squirrel monkey. J. Neurosci 13, 1120–1137. [PubMed: 7680067]

Haber SN, Kunishio K, Mizobuchi M, Lynd-Balta E, 1995. The orbital and medial prefrontal circuit through the primate basal ganglia. J. Neurosci 15, 4851–4867. [PubMed: 7623116]

Desban M, Gauchy C, Glowinski J, Kemel ML, 1995. Heterogeneous topographical distribution of the striatonigral and striatopallidal neurons in the matrix compartment of the cat caudate nucleus. J. Comp. Neurol 352, 117–133. [PubMed: 7536221]

Lopez-Figueroa MO, Ramirez-Gonzalez JA, Divac I, 1995. Projections from the visual areas to the neostriatum in rats. A re-examination. Acta Neurobiol. Exp 55, 165–175 (Wars).

Deschenes M, Bourassa J, Doan VD, Parent A, 1996. A single-cell study of the axonal projections arising from the posterior intralaminar thalamic nuclei in the rat. Eur. J. Neurosci 8, 329–343. [PubMed: 8714704]

Inase M, Sakai ST, Tanji J, 1996. Overlapping corticostriatal projections from the supplementary motor area and the primary motor cortex in the macaque monkey: an anterograde double labeling study. J. Comp. Neurol 373, 283–296. [PubMed: 8889928]

Kincaid AE, Wilson CJ, 1996. Corticostriatal innervation of the patch and matrix in the rat neostriatum. J. Comp. Neurol 374, 578–592. [PubMed: 8910736]

Funaki S, Meguro R, Abe H, Norita M, 1998. The organization of the thalamostriatal projection from the lateral posterior thalamic nuclear complex (LP) in the pigmented rat. Neurobiology 6, 273–294 (Bp). [PubMed: 9778648]

Nisenbaum LK, Webster SM, Chang SL, McQueeney KD, LoTurco JJ, 1998. Early patterning of prelimbic cortical axons to the striatal patch compartment in the neonatal mouse. Dev. Neurosci 20, 113–124. [PubMed: 9691187]

Reep RL, Cheatwood JL, Corwin JV, 2003. The associative striatum: organization of cortical projections to the dorsocentral striatum in rats. J. Comp. Neurol 467, 271–292. [PubMed: 14608594]

Cheatwood JL, Corwin JV, Reep RL, 2005. Overlap and interdigitation of cortical and thalamic afferents to dorsocentral striatum in the rat. Brain Res. 1036, 90–100. [PubMed: 15725405]

Avendano C, de Las Heras S, Gimenez-Amaya JM, 2006. Striatal projections from the lateral and posterior thalamic complexes. An anterograde tracer study in the cat. Histochem. Cell Biol 125, 265–271. [PubMed: 16195893]

Kamishina H, Yurcisin GH, Corwin JV, Reep RL, 2008. Striatal projections from the rat lateral posterior thalamic nucleus. Brain Res. 1204, 24–39. [PubMed: 18342841]

Day-Brown JD, Wei H, Chomsung RD, Petry HM, Bickford ME, 2010. Pulvinar projections to the striatum and amygdala in the tree shrew. Front. Neuroanat 4, 143. [PubMed: 21120139]

Unzai T, Kuramoto E, Kaneko T, Fujiyama F, 2015. Quantitative analyses of the projection of individual neurons from the midline thalamic nuclei to the striosome and matrix compartments of the rat striatum. Cereb. Cortex

Perlis RH, 2008. Association of a polymorphism near CREB1 with differential aversion processing in the insula of healthy participants. Arch. Gen. Psychiatry 65, 882–892. [PubMed: 18678793]

Kim BW, 2010. Recurrent, robust and scalable patterns underlie human approach and avoidance. PLoS One 5, e10613. [PubMed: 20532247]

Blood AJ, 2012. Evidence for altered basal ganglia-brainstem connections in cervical dystonia. PLoS One 7, e31654. [PubMed: 22384048]

Waugh JL, 2016. Thalamic volume is reduced in cervical and laryngeal dystonias. PLoS One 11, e0155302. [PubMed: 27171035]

Bruggemann N, 2016. Neuroanatomical changes extend beyond striatal atrophy in X-linked dystonia parkinsonism. Parkinsonism Relat. Disord 31, 91–97. [PubMed: 27481033]

Hanssen H, 2018. Basal ganglia and cerebellar pathology in X-linked dystonia-parkinsonism. Brain 141, 2995–3008. [PubMed: 30169601]

Waugh JL, 2019. A registration method for improving quantitative assessment in probabilistic diffusion tractography. Neuroimage 189, 288–306. [PubMed: 30611874]

van der Kouwe AJ, 2005. On-line automatic slice positioning for brain MR imaging. Neuroimage 27, 222–230. [PubMed: 15886023]

Talairach J, Tournoux P, 1988. Co-Planar Stereotaxic Atlas of the Human Brain: 3-D Proportional System: An Approach to Cerebral Imaging. Thieme.

White LE, 1997. Structure of the human sensorimotor system. I: morphology and cytoarchitecture of the central sulcus. Cereb. Cortex 7, 18–30. [PubMed: 9023429]

Picard N, Strick PL, 2001. Imaging the premotor areas. Curr. Opin. Neurobiol 11, 663–672. [PubMed: 11741015]

Chouinard PA, Paus T, 2006. The primary motor and premotor areas of the human cerebral cortex. Neuroscientist 12, 143–152. [PubMed: 16514011]

Behrens TE, Berg HJ, Jbabdi S, Rushworth MF, Woolrich MW, 2007. Probabilistic diffusion tractography with multiple fibre orientations: what can we gain? Neuroimage 34, 144–155. [PubMed: 17070705]

Johnston JG, Gerfen CR, Haber SN, van der Kooy D, 1990. Mechanisms of striatal pattern formation: conservation of mammalian compartmentalization. Brain Res. Dev. Brain Res 57, 93–102. [PubMed: 1965303]

Desikan RS, 2006. An automated labeling system for subdividing the human cerebral cortex on MRI scans into gyral based regions of interest. Neuroimage 31, 968–980. [PubMed: 16530430]

Lancaster JL, 2000. Automated Talairach atlas labels for functional brain mapping. Hum. Brain Mapp 10, 120–131. [PubMed: 10912591]

Phillips JM, 2019. Topographic organization of connections between prefrontal cortex and mediodorsal thalamus: evidence for a general principle of indirect thalamic pathways between directly connected cortical areas. Neuroimage 189, 832–846. [PubMed: 30711468]

Ender P, 2021. How Can I do Tests of Simple Main Effects in Stata?. Institute for Digital Research and Education, UCLA).

Benjamini Y, Hochberg Y, 1995. Controlling the false discovery rate: a practical and powerful approach to multiple testing. J. R. Stat. Soc. Ser. B 57, 289–300 (Methodological).

Saint-Cyr JA, Ungerleider LG, Desimone R, 1990. Organization of visual cortical inputs to the striatum and subsequent outputs to the pallido-nigral complex in the monkey. J. Comp. Neurol 298, 129–156. [PubMed: 1698830]

Weiss AR, Liguore WA, Domire JS, Button D, McBride JL, 2020. Intra-striatal AAV2.retro administration leads to extensive retrograde transport in the rhesus macaque brain: implications for disease modeling and therapeutic development. Sci. Rep 10, 6970. [PubMed: 32332773]

McFarland NR, Haber SN, 2000. Convergent inputs from thalamic motor nuclei and frontal cortical areas to the dorsal striatum in the primate. J. Neurosci 20, 3798–3813. [PubMed: 10804220]

Takada M, 2001. Organization of inputs from cingulate motor areas to basal ganglia in macaque monkey. Eur. J. Neurosci 14, 1633–1650. [PubMed: 11860458]

Goldman-Rakic PS, Porrino LJ, 1985. The primate mediodorsal (MD) nucleus and its projection to the frontal lobe. J. Comp. Neurol 242, 535–560. [PubMed: 2418080]

Vogt BA, Pandya DN, Rosene DL, 1987. Cingulate cortex of the rhesus monkey: I. Cytoarchitecture and thalamic afferents. J. Comp. Neurol 262, 256–270. [PubMed: 3624554]

van Vulpen EH, Verwer RW, 1989. Organization of projections from the mediodorsal nucleus of the thalamus to the basolateral complex of the amygdala in the rat. Brain Res. 500, 389–394. [PubMed: 2605505]

O'Muircheartaigh J, Keller SS, Barker GJ, Richardson MP, 2015. White matter connectivity of the thalamus delineates the functional architecture of competing thalamocortical systems. Cereb. Cortex 25, 4477–4489. [PubMed: 25899706]

Tziortzi AC, 2014. Connectivity-based functional analysis of dopamine release in the striatum using diffusion-weighted MRI and positron emission tomography. Cereb. Cortex 24, 1165–1177. [PubMed: 23283687]

Schilling KG, 2019. Limits to anatomical accuracy of diffusion tractography using modern approaches. Neuroimage 185, 1–11. [PubMed: 30317017]

Norden JJ, Lin CS, Kaas JH, 1978. Subcortical projections of the dorsomedial visual area (DM) of visual association cortex in the owl monkey, Aotus trivirgatus. Exp. Brain Res 32, 321–334. [PubMed: 98340]

Campos-Ortega JA, 1968. Descending subcortical projections from the occipital lobe of Galago crassicaudatus. Exp. Neurol 21, 440–454. [PubMed: 4877899]

Gattass R, Galkin TW, Desimone R, Ungerleider LG, 2014. Subcortical connections of area V4 in the macaque. J. Comp. Neurol 522, 1941–1965. [PubMed: 24288173]

Maioli MG, Squatrito S, Battaglini PP, Rossi R, Galletti C, 1983. Projections from the visual cortical region of the superior temporal sulcus to the striatum and claustrum in the macaque monkey. Arch. Ital. Biol 121, 259–266. [PubMed: 6675533]

Ungerleider LG, Desimone R, Galkin TW, Mishkin M, 1984. Subcortical projections of area MT in the macaque. J. Comp. Neurol 223, 368–386. [PubMed: 6323553]

Webster MJ, Bachevalier J, Ungerleider LG, 1993. Subcortical connections of inferior temporal areas TE and TEO in macaque monkeys. J. Comp. Neurol 335, 73–91. [PubMed: 8408774]

Yeterian EH, Pandya DN, 1995. Corticostriatal connections of extrastriate visual areas in rhesus monkeys. J. Comp. Neurol 352, 436–457. [PubMed: 7706560]

Weller RE, Steele GE, Kaas JH, 2002. Pulvinar and other subcortical connections of dorsolateral visual cortex in monkeys. J. Comp. Neurol 450, 215–240. [PubMed: 12209852]

Carman JB, Cowan WM, Powell TP, 1963. The organization of cortico-striate connexionsin the rabbit. Brain 86, 525–562. [PubMed: 14063897]

Webster KE, 1965. The cortico-striatal projection in the cat. J. Anat 99, 329–337. [PubMed: 14327177]

Graham J, Lin CS, Kaas JH, 1979. Subcortical projections of six visual cortical areas in the owl monkey, Aotus trivirgatus. J. Comp. Neurol 187, 557–580. [PubMed: 114555]

Ungerleider LG, Galkin TW, Desimone R, Gattass R, 2014. Subcortical projections of area V2 in the macaque. J. Cogn. Neurosci 26, 1220–1233. [PubMed: 24456395]

Ogawa A, 2018. Striatal subdivisions that coherently interact with multiple cerebrocortical networks. Hum Brain Mapp 39, 4349–4359. [PubMed: 29975005]

Liu X, 2020. Joint multi-modal parcellation of the human striatum: functions and clinical relevance. Neurosci. Bull 36, 1123–1136. [PubMed: 32700142]

Ramos-Llorden G, 2020. High-fidelity, accelerated whole-brain submillimeter *in vivo* diffusion MRI using gSlider-spherical ridgelets (gSlider-SR). Magn. Reson. Med. official journal of the Society of Magnetic Resonance in Medicine /Society of Magnetic Resonance in Medicine

Levesque M, Parent A, 1998. Axonal arborization of corticostriatal and corticothalamic fibers arising from prelimbic cortex in the rat. Cereb. Cortex 8, 602–613. [PubMed: 9823481]

Morton AJ, Nicholson LF, Faull RL, 1993. Compartmental loss of NADPH diaphorase in the neuropil of the human striatum in Huntington's disease. Neuroscience 53, 159–168. [PubMed: 7682296]

Goto S, 2005. Functional anatomy of the basal ganglia in X-linked recessive dystonia–parkinsonism. Ann. Neurol 58, 7–17. [PubMed: 15912496]

Lawhorn C, Smith DM, Brown LL, 2009. Partial ablation of mu-opioid receptor rich striosomes produces deficits on a motor-skill learning task. Neuroscience 163, 109–119. [PubMed: 19463902]

Friedman A, 2015. A corticostriatal path targeting striosomes controls decision-making under conflict. Cell 161, 1320–1333. [PubMed: 26027737]

Saka E, Goodrich C, Harlan P, Madras BK, Graybiel AM, 2004. Repetitive behaviors in monkeys are linked to specific striatal activation patterns. J. Neurosci 24, 7557–7565. [PubMed: 15329403]

Canales JJ, Graybiel AM, 2000. A measure of striatal function predicts motor stereotypy. Nat. Neurosci 3, 377–383. [PubMed: 10725928]

Graybiel AM, Moratalla R, Robertson HA, 1990. Amphetamine and cocaine induce drug-specific activation of the c-fos gene in striosome-matrix compartments and limbic subdivisions of the striatum. Proc. Natl. Acad. Sci. U. S. A 87, 6912–6916. [PubMed: 2118661]

Granado N, 2010. Selective vulnerability in striosomes and in the nigrostriatal dopaminergic pathway after methamphetamine administration : early loss of TH in striosomes after methamphetamine. Neurotox Res. 18, 48–58. [PubMed: 19760475]

Granado N, Escobedo I, O'Shea E, Colado I, Moratalla R, 2008. Early loss of dopaminergic terminals in striosomes after MDMA administration to mice. Synapse 62, 80–84. [PubMed: 17960765]

Huntley ED, 2020. Adolescent substance use and functional connectivity between the ventral striatum and hippocampus. Behav. Brain Res 112678. [PubMed: 32413469]
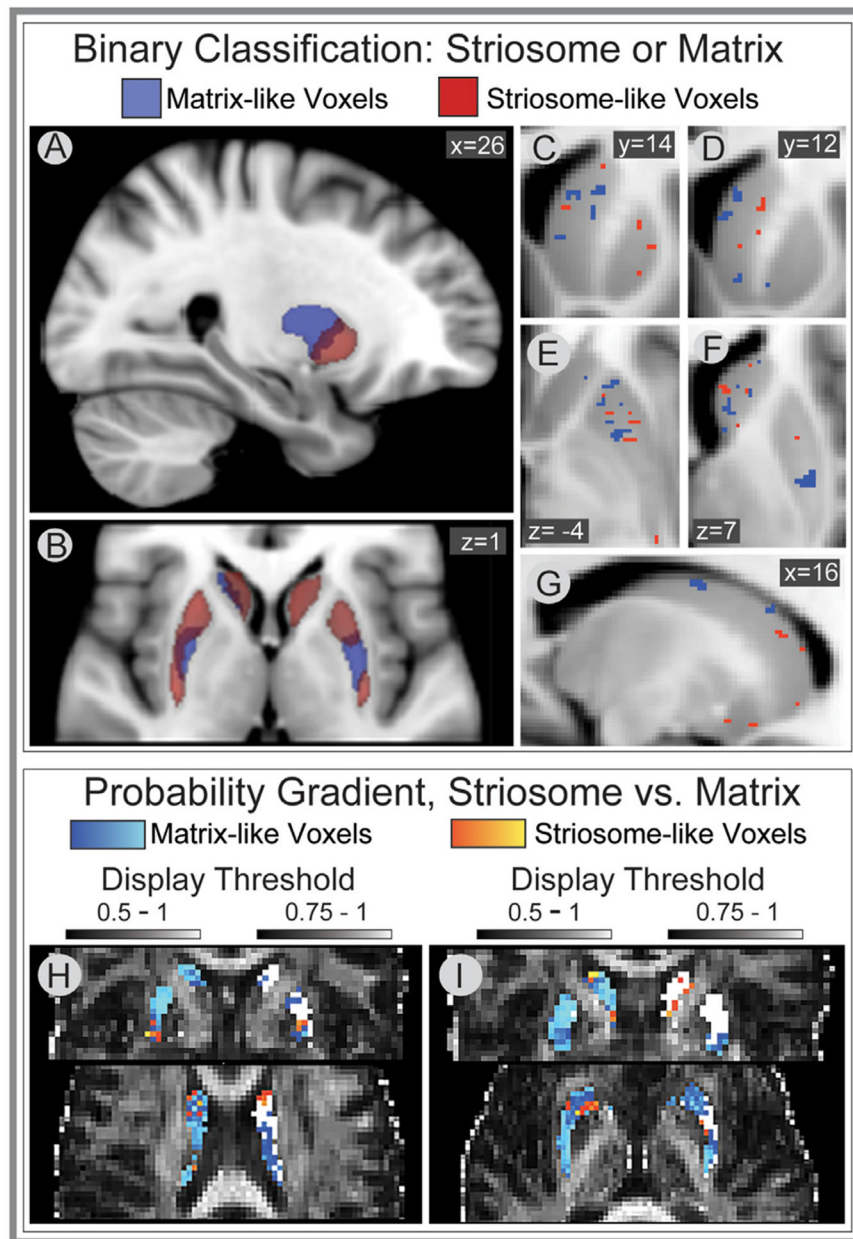
Fig. 1.
Anatomical distribution of matrix-like and striosome-like voxels. The anatomical distribution of matrix-like and striosome-like voxels determined by classification targets tractography (CTT) mirrors the location of matrix and striosomes identified by prior histologic studies. In sagittal (A) and axial (B) views of the human striatum, average CTT results illustrate the probability of connection with matrix-like (blue) or striosome-like (red) cortical targets. CTT values >50% indicate a "win" for one compartment, with increasing percentiles reflecting higher certainty that a given voxel has a matrix-like or striosome-like pattern of connectivity. CTT images are displayed with threshold 40–100% to demonstrate the overlap in connectivity for marginal voxels, and are overlaid on the MNI_152_1 mm template brain. Striosome-like voxels were significantly more likely to

be found in rostroventral sites (four-factor ANOVA, rostral-caudal axis $(F(2, 122)=6.23,$ $p < 0.00001)$ and dorsal-ventral axis $(F(2, 122)=3.98, p < 0.00001))$. However, as in human and animal histology, single matrix-like and striosome-like voxels may be found at virtually every point in the striatum. Striata of single participants (panels C–G) illustrate that matrix-like and striosome-like voxels are distributed uniquely in each individual. Each colored voxel in C–G was selected individually by algorithm, not as part of a cluster, and is among the most-biased voxels in the probability distribution (lying in the tails beyond the central 1.5SD of all voxels). Coordinates follow MNI convention. While panels C–G demonstrate the striatal voxels with the greatest bias toward one compartment, the majority of striatal voxels have only moderate compartment-specific bias. In two individual subjects (H, I), coronal (above) and axial (below) views of the same tractography-based probability distribution are displayed. For both subjects, the right hemisphere is displayed with a threshold of 0.5–1, such that every voxel includes a probability estimate, to give readers information about the spatial pattern of matrix and striosome in the human. In contrast, the left hemisphere is displayed with a threshold of 0.75–1, masking voxels with middling bias in connectivity and revealing the striatal seed mask (white voxels) behind the probability distribution. Probability distributions are overlaid on each individual's FA image. The probability distributions for individual subjects follow the same trends as the group average – striosome-like voxels are more likely to be located in the rostroventral striatum, while matrix-like voxels may be found in every part of the striatum.
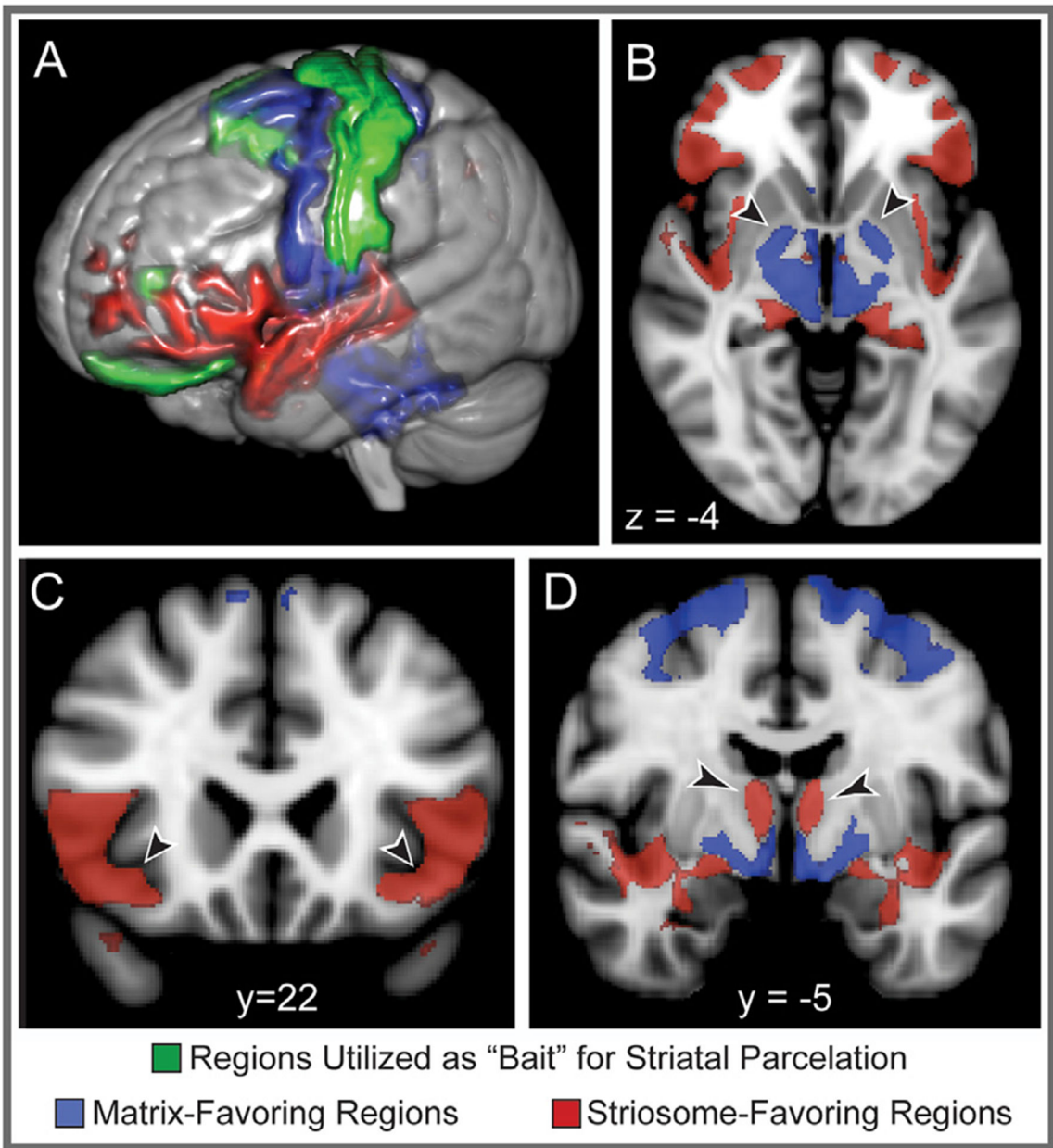
Fig. 2. Whole brain tractography utilizing parcellated striatal compartments as targets.
After striatal voxels were identified as striosome-like or matrix-like by differential preference tractography, those voxels then served as compartment-specific target masks for whole brain tractography. Brain regions that do not exist in experimental animals, and regions that were never reported in prior animal tract tracing studies, could thereby be identified as having striosome-favoring or matrix-favoring patterns of connectivity. In A, connectivity with "bait" regions (left hemisphere, green) predicts patterns of connectivity with both contiguous and remote voxels. This allowed us to identify regions with highly biased connectivity for subsequent experiments (arrowheads): globus pallidus interna (B), basal operculum (C), and mediodorsal thalamus (D). Average connectivity for each voxel is overlaid on the MNI152_T1_1 mm standard brain. Coordinates follow MNI convention.
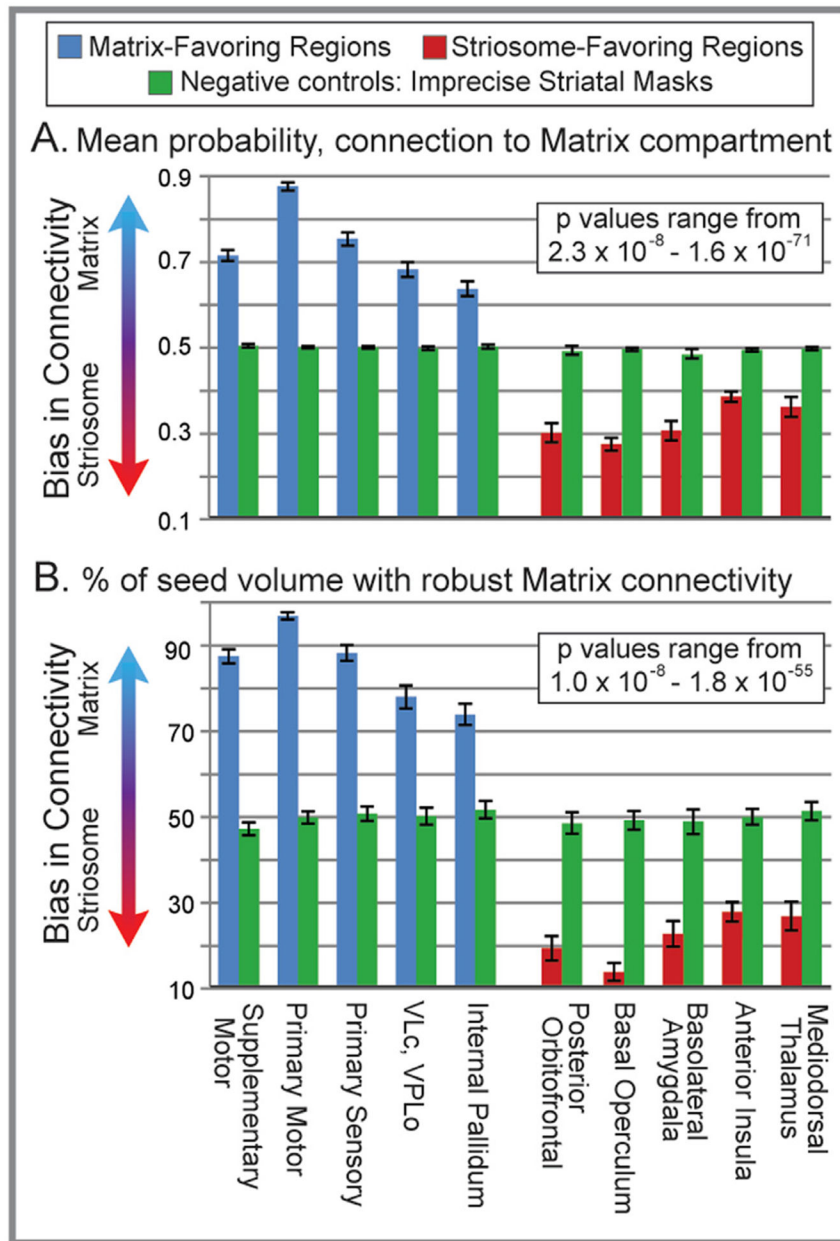
Fig. 3.

Quantitative tractography confirms the compartment selectivity demonstrated in animal injectable tracer studies. Matrix-like and striosome-like voxels have highly segregated patterns of structural connectivity. We identified 10 regions whose projections to the matrix or striosome compartments were highly segregated in both animal tract tracing studies and our imaging parcellation method. For each comparison, we defined the striatal compartments using nine gray matter regions, and tested the strength of connectivity with the tenth, elided region (known here as "N-1 analyses"). The mean connectivity to the matrix-like compartment (A) assessed the general strength of discrimination between the striatal compartments. To assess for local maxima of connectivity preference, we determined the percentage of all voxels exceeding a connectivity threshold (>1.5SD) that

were biased toward the matrix-like compartment (B). For both quantification methods, our classification targets tractography method robustly categorized each region as matrix-favoring or striosome-favoring in a pattern identical to that demonstrated by prior animal tract tracing studies. Deviation from chance (50%) indicates a connectivity bias toward one striatal compartment: blue bars for matrix-favoring regions, red bars for striosome-favoring regions. When striatal masks were placed without regard to extra-striate connectivity (checkerboard masks, negative control, green bars) all regional bias for one striatal compartment was abolished. Data from left hemisphere regions is shown; results from the right hemisphere were highly similar. Multiple comparisons correction, Benjamini-Hochberg procedure, yielded a corrected significance threshold of $p < 2.5 \times 10^{-2}$ for measures of connection probability (A) and $p < 4.12 \times 10^{-2}$ for volumetric measures (B). Error bars represent the standard error of the mean.
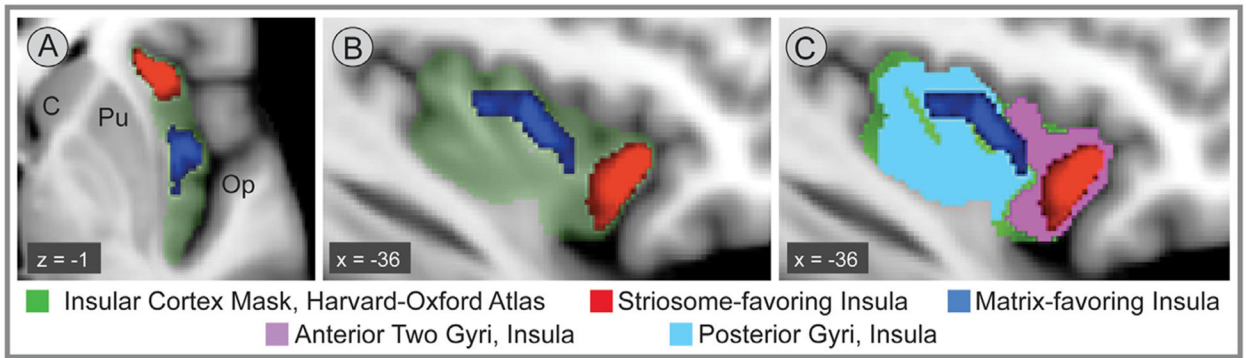
Fig. 4.
Somatotopic organization of striosome-like voxels. Striosome-like voxels are organized somatotopically, with connectivity dominated by a particular striosome-favoring region (colored voxels) in distinct parts of the striatum. The average probability distribution for all 122 participants is shown in the left-hand panels (right hemisphere, A, D, G), while the center and right-hand panels (left hemisphere) show probability distributions for individual participants relative to the MNI152_T1_1 mm standard brain. Distributions in the coronal (panels A–C), axial (panels D–F) and sagittal (panels G–I) planes illustrate the somatotopic organization of projections to striosomes. Note that while individuals differ in the precise sites of striosome-like voxels (center and right columns), all panels illustrate the trend for segmentation into region-specific zones. These zones do not imply that a given region only connects with striosomes in that area, or that striosomes in that area connect only with the dominant region; rather, in these zones a particular region has stronger influence on striosome-like identity than other striosome-favoring regions. Images are displayed by radiographic convention, with the left hemisphere on the right side of the image. Coordinates follow MNI convention. Abbreviations: Ca, Caudate; Pu, Putamen.
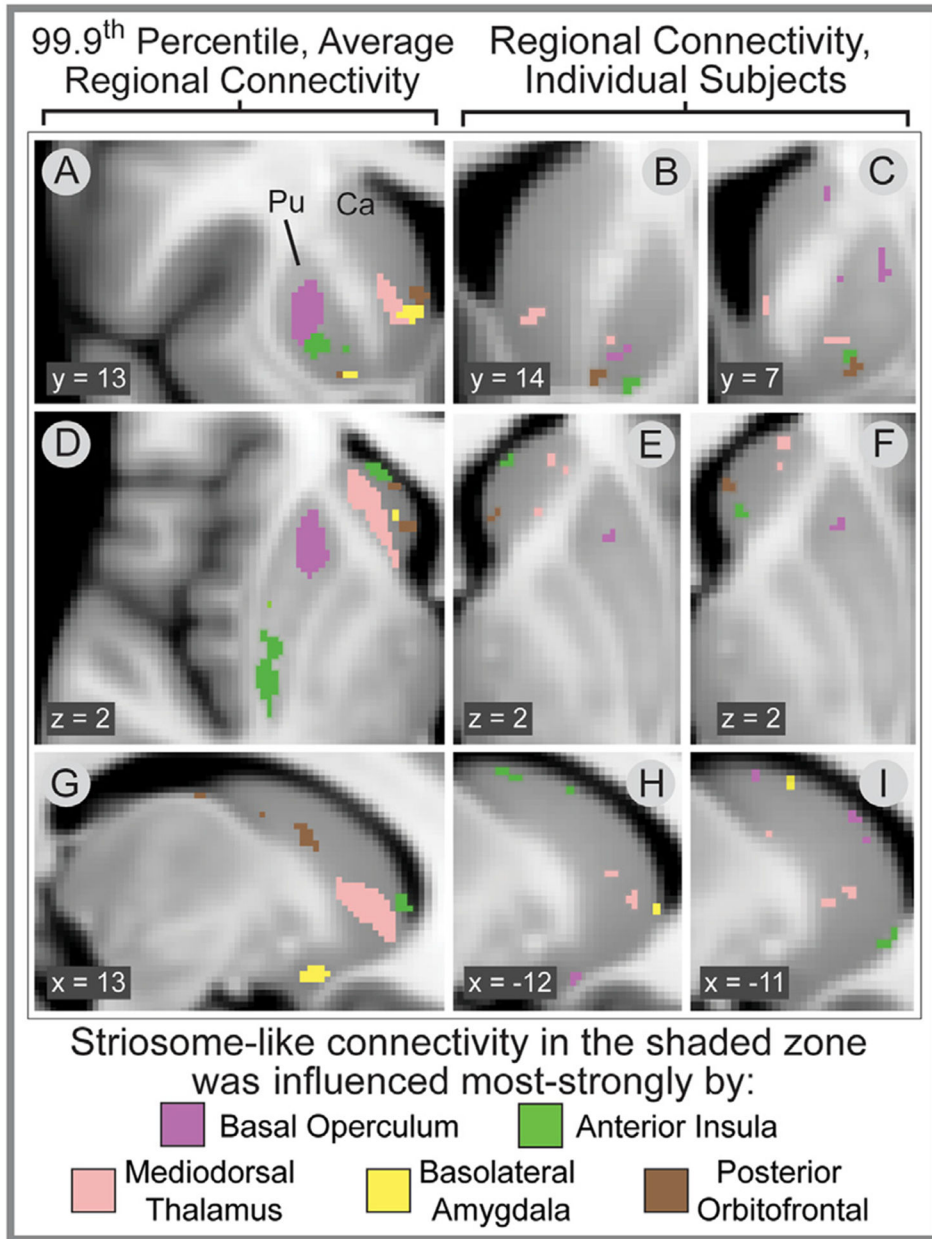
Fig. 5.

Mixed striatal selectivity in insular cortex. Striosome-favoring voxels (red) are concentrated in the anterior and postero-lateral insula (latter not shown in this view), while matrix-favoring voxels (navy blue) are found primarily in the centrosuperior insula (average profiles of 122 participants, left insula). The Insular Cortex mask (green, derived from the Harvard-Oxford Cortical Atlas) is anatomically accurate but blends subregions with opposite striatal projection patterns. Segregating the insula by gyri (anterior two, purple, vs all posterior, light blue) aligns the anatomical masks with prior animal tract tracing literature. Mean connectivity, whole Insular Cortex: 51.4% striosome, NS; anterior insula, 73.6% striosome, $p < 1.90 \times 10^{-18}$; posterior insula, 62.7% matrix, $p < 7.49 \times 10^{-5}$; significance threshold, $p <$

4.12×10^{-2}). Coordinates follow MNI convention. Abbreviations: C, caudate; Pu, putamen; Op, operculum.
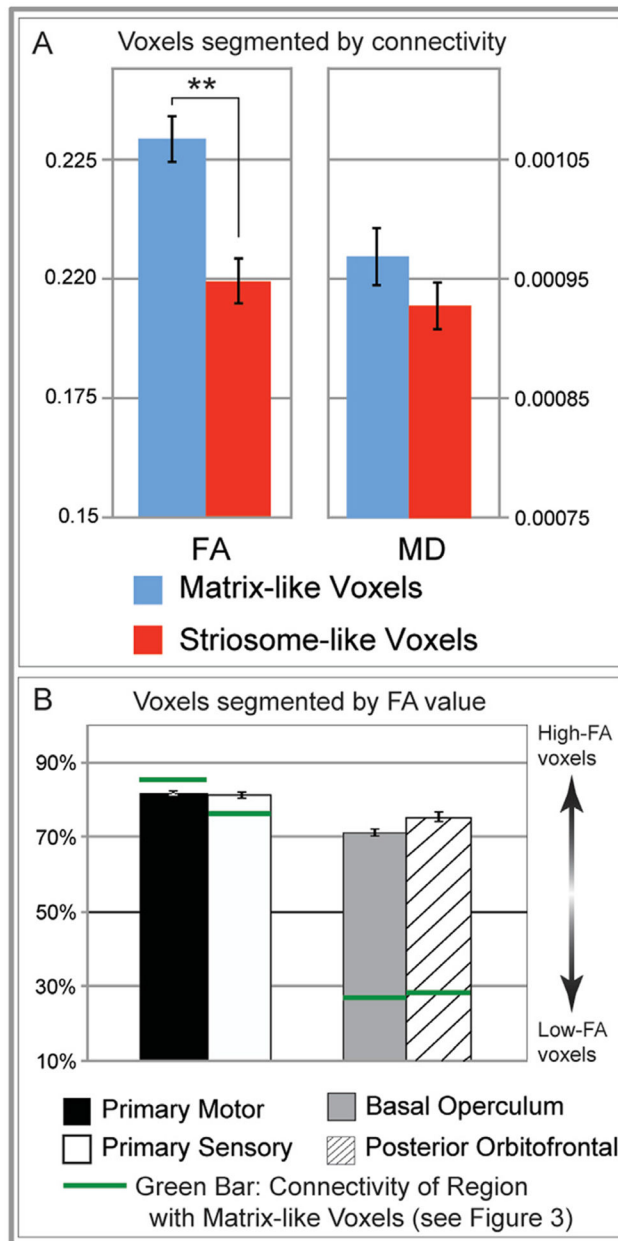
Fig. 6.
Striosome-like and matrix-like voxels differ in diffusion properties. A measure of tissue microstructure (fractional anisotropy, FA) in striatal voxels differs between striosome-like and matrix-like compartments, but FA differences do not drive biased connectivity. In A, (FA is significantly lower in striosome-like voxels, while mean diffusivity (MD) did not differ between striosome-like and matrix-like compartments (combined hemispheres). Paired-samples t-test, Bonferroni corrected; **, $p < 3.4 \times 10^{-9}$. In B, we tested whether differences in mean FA were the drivers of biased striatal connectivity. Rather than parcellating the striatum by connectivity (as in A and in other Figures), here we parcellated the striatum by selecting high- and low-FA voxels. Using these FA-parcellated striatal voxels as targets and using the two matrix-favoring and two striosome-favoring regions with the

largest biases in connectivity (N-1 experiments, Fig. 3) as seeds, we assessed the impact of FA on compartment-biased connectivity. All regions were strongly biased towards high-FA voxels, even those regions whose connectivity favors striosomes (low-FA, basal operculum and posterior orbitofrontal). Matrix-favoring regions (primary motor and sensory) lost the precision seen with connectivity-based striatal parcellation. Green bars indicate the bias in connectivity demonstrated in the N-1 experiments, combined hemispheres. For both A and B, error bars represent the standard error of the mean.
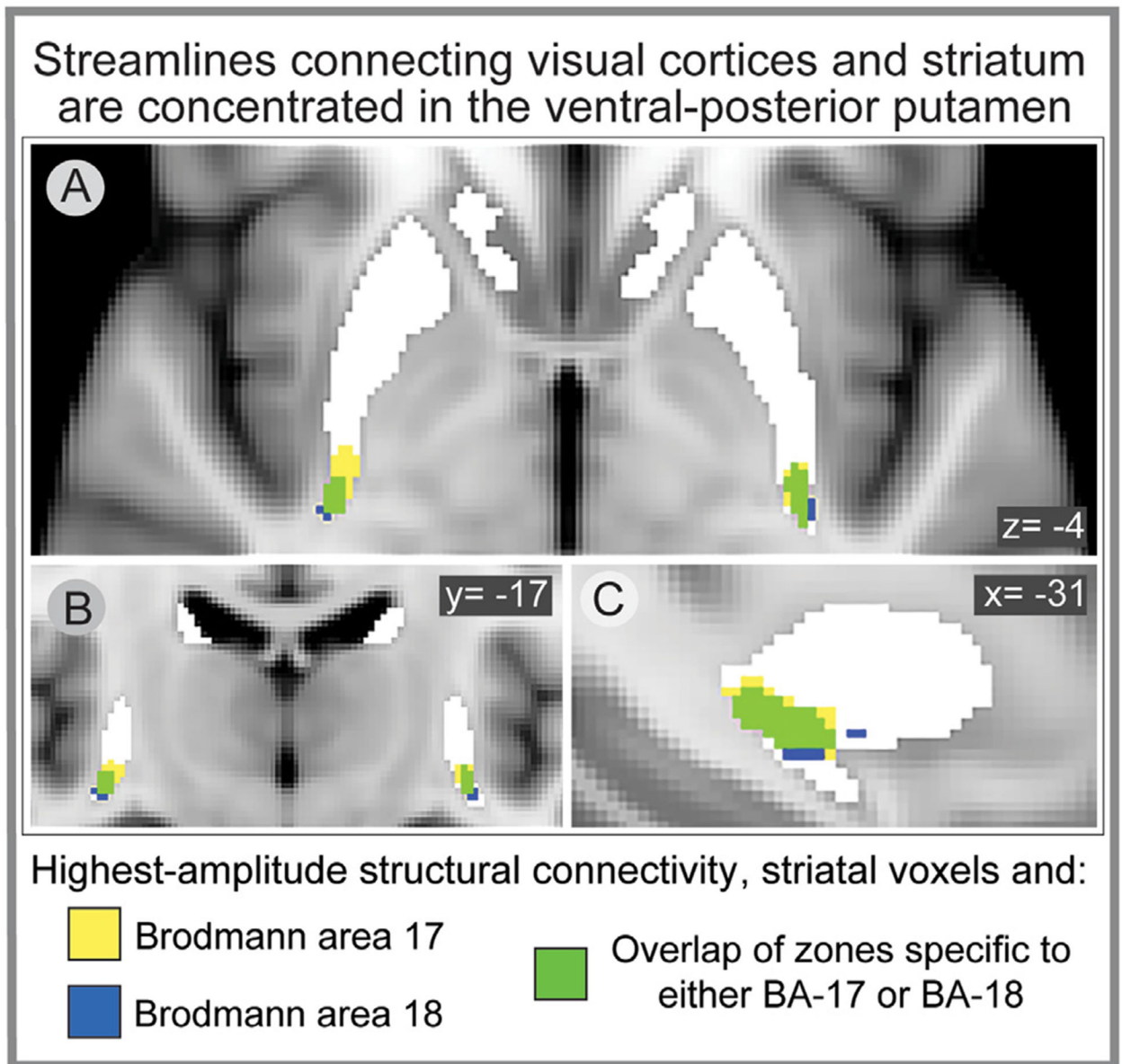
Fig. 7.
Occipitostriate projections. Diffusion streamlines connecting visual cortices and the striatum are concentrated in the ventral-posterior putamen (VPP). Classification targets tractography (CTT) considered each striatal voxel as an independent seed with the potential to project to single targets (Brodmann area 17 or 18, assessed in separate rounds of CTT). As seen in axial (A, $z = -4$), coronal (B, $y = -17$), and sagittal (C, left hemisphere, $x = -31$) views, projections from these occipital regions to the striatum are highly concentrated in the VPP. While projections from Brodmann areas 17 and 18 have distinct areas of concentration (yellow and blue voxels, respectively), their areas of enriched connectivity mostly overlap (green voxels). The VPP also overlaps with the striatal targets of projections from other (non-primary) visual areas, as demonstrated by tract tracing studies in primates. Most regions of the striatum (white voxels) had only low-amplitude, non-specific connectivity

with Brodmann areas 17 and 18. Note that we excluded the nucleus accumbens for all striatal parcellations presented herein, which is why the medial portions of the head of the caudate appear eroded (A, center of image). Striatal volumes are projected on the MNI152_T1_1 mm template brain.

Table 1

(A and B) – Biased striatal connectivity among the brain regions of the Harvard-Oxford Atlas. Table 1: We measured connectivity with striatal compartments in regions of interest (ROI) from the Harvard-Oxford cortical and subcortical atlases (HOA). ROI numbers correspond to the enumeration of the HOA Cortical atlas, while ROIs beginning with "S-" correspond to the HOA Subcortical atlas. Regions connecting with matrix and striosome are listed in A and B, respectively. Regions included here were biased towards one striatal compartment for at least one hemisphere; in no case did biased regional connectivity differ between hemispheres. As measured by the percentage of all supra-threshold voxels projecting to the dominant compartment, or by the fold-increase in the number of individual participants having very strong (>95%) connectivity to the dominant compartment ($N_{dominant}:N_{nondominant}$), most brain regions have a clear pattern of bias in their structural connectivity. Regions in which prior studies conflicting compartment preference are indicated by "Mixed." Family-wise error rate corrected using the Benjamini-Hochberg procedure, yielding adjusted significance threshold $p < 4.12 \times 10^{-2}$ (*). ROIs with $p < 4.12 \times 10^{-11}$ are indicated by **. Note that a parallel and more granular set of analyses, extracted via the regions of the Talairach brain atlas, can be seen in Supplemental Table 2.

A

HOA ROI #	Region	Hemi-sphere	% of Voxels to Matrix Compartment	p-value	X-Fold Increase Over Striosome Compartment	Concurs with Animal Tract-Tracing Studies	Region Never Reported in Animals
				Matrix-favoring Regions			
2	Superior Frontal Gyrus	L	75.3	5.62×10^{-19}**	43	X	
		R	82.5	4.85×10^{-31}**	54		
3	Middle Frontal Gyrus	L	78.8	3.47×10^{-9}*	1.5	X	
		R	86.9	1.55×10^{-40}**	67		
5	Inferior Frontal Gyrus, pars opercularis	L	69	2.98×10^{-9}*	5.8		X
		R	78.6	5.11×10^{-18}**	6.7		
6	Precentral Gyrus	L	95.8	4.49×10^{-79}**	98	X	
		R	97.7	1.63×10^{-120}**	106		
12	Middle Temporal Gyrus, temporooccipital part	L	60.4	6.19×10^{-3}*	1.7		X
		R	72.1	1.36×10^{-10}*	4.1		
16	Postcentral Gyrus	L	82.5	7.98×10^{-29}**	31	X	
		R	84.6	4.71×10^{-32}**	22		
17	Superior Parietal Lobule	L	83.4	1.17×10^{-24}**	15	X	
		R	85.8	1.31×10^{-37}**	71		
18	Supramarginal Gyrus, anterior division	L	78.3	5.02×10^{-16}**	16		X

A

HOA ROI #	Region	Hemi-sphere	% of Voxels to Matrix Compartment	p-value	X-Fold Increase Over Striosome Compartment	Concurs with Animal Tract-Tracing Studies	Region Never Reported in Animals
19	Supramarginal Gyrus, posterior division	R	84.2	3.21×10^{-26}**	18		
		L	71.4	5.47×10^{-9}*	5.1		X
20	Angular Gyrus	R	79.6	1.52×10^{-21}**	27		
		L	71.8	1.74×10^{-9}*	5.1		X
25	Juxtapositional Lobule Cortex (formerly SMA)	R	82.9	2.54×10^{-29}**	57		
		L	91.3	6.97×10^{-53}**	87	X	
41	Central Opercular Cortex	R	94.3	1.41×10^{-65}**	95		
		L	71.5	9.39×10^{-11}*	8.5		X
42	Parietal Operculum Cortex	R	75.8	3.10×10^{-15}**	5.6		
		L	57.6	6.18×10^{-2}	1.5		X
S-6	Pallidum	R	64.3	1.55×10^{-4}*	2.9		
		L	71.6	6.83×10^{-22}**	6	X	
S-17		R	68.8	4.52×10^{-19}**	12		

B

HOA ROI #	Region	Hemi-sphere	% of Voxels to Striosome Compartment	p-value	X-Fold Increase Over Matrix Compartment	Concurs with Animal Tract-Tracing Studies	Region Never Reported in Animals
				Striosome-favoring Regions			
0	Frontal Pole	L	75.8	1.13×10^{-20}**	36	X - Mixed	
		R	70.8	1.30×10^{-14}**	26		
1	Insular Cortex	L	51.4	5.85×10^{-1}	20	X	
		R	57.6	7.06×10^{-3}*	5		
4	Inferior Frontal Gyrus, pars triangularis	L	66.7	3.76×10^{-8}**	6.5		X
		R	56.1	6.52×10^{-2}	1.6		
7	Temporal Pole	L	73.8	6.83×10^{-11}*	5.3		X
		R	79.2	1.16×10^{-17}**	6.8		
8	Superior Temporal Gyrus, anterior division	L	62.5	1.68×10^{-3}*	1.9		X
		R	66.5	2.15×10^{-5}*	2.3		
10	Middle Temporal Gyrus, anterior division	L	66.4	2.95×10^{-4}*	2.8		X

A

HOA ROI #	Region	Hemisphere	% of Voxels to Matrix Compartment	p-value	X-Fold Increase Over Striosome Compartment	Concurs with Animal Tract-Tracing Studies	Region Never Reported in Animals
13	Inferior Temporal Gyrus, anterior division	R	69.5	4.44×10^{-7}*	3.3		
		L	70.5	1.26×10^{-7}*	3.4		X
14	Inferior Temporal Gyrus, posterior division	R	74.4	2.07×10^{-10}*	4.9		
		L	67.7	8.29×10^{-7}*	3.8		X
15	Inferior Temporal Gyrus, temporooccipital part	R	62.8	2.67×10^{-4}*	3.7		
		L	61.2	2.01×10^{-3}*	2.4		X
22	Lateral Occipital Cortex, inferior division	R	59.1	1.41×10^{-2}*	2.3		
		L	62.4	6.32×10^{-4}*	2		X
23	Intracalcarine Cortex	R	62	5.66×10^{-4}*	2.4		
		L	82.4	6.85×10^{-23}**	22	Opposite	
24	Frontal Medial Cortex	R	85.4	3.40×10^{-27}**	20		
		L	67.8	2.60×10^{-6}*	3.6	X	
26	Subcallosal Cortex	R	75.1	1.37×10^{-12}**	7.2		
		L	61.6	2.95×10^{-3}*	2.2	X	
27	Paracingulate Gyrus	R	71.1	9.17×10^{-9}*	4.8		
		L	61.5	1.68×10^{-4}*	3.7		X
28	Anterior Cingulate Gyrus	R	55.9	7.79×10^{-2}	1.4		
		L	59.5	1.23×10^{-3}*	4.5	X	
30	Precuneous Cortex	R	51	7.50×10^{-1}	1.6		
		L	50.7	8.24×10^{-1}	1.5		X
31	Cuneal Cortex	R	56.7	3.43×10^{-2}*	1.2		
		L	75.2	3.12×10^{-12}**	7.2	X - Mixed	
32	Frontal Orbital Cortex	R	80.8	1.46×10^{-20}**	19		
		L	84.4	3.62×10^{-33}**	69	X	
33	Parahippocampal Gyrus, anterior division	R	83.2	1.99×10^{-28}**	67		
		L	66.8	4.21×10^{-7}*	2.8		X
34	Parahippocampal Gyrus, posterior division	R	79.5	8.27×10^{-19}**	11		
		L	68.3	1.56×10^{-8}*	4.1		X

A

HOA ROI #	Region	Hemi-sphere	% of Voxels to Matrix Compartment	p-value	X-Fold Increase Over Striosome Compartment	Concurs with Animal Tract-Tracing Studies	Region Never Reported in Animals
35	Lingual Gyrus	R	77.2	1.73×10^{-18}**	19		
		L	73.3	7.59×10^{-11}*	3.8	X - Mixed	
36	Temporal Fusiform Cortex, anterior division	R	71.4	1.40×10^{-9}*	8.7		
		L	76.4	6.86×10^{-13}**	4.7		X
37	Temporal Fusiform Cortex, posterior division	R	79.1	1.04×10^{-15}**	8.4		
		L	80.1	2.72×10^{-20}**	12		X
38	Temporal Occipital Fusiform Cortex	R	82.1	2.51×10^{-24}**	23		
		L	68	1.27×10^{-6}*	3.3		X
39	Occipital Fusiform Gyrus	R	73.8	8.49×10^{-12}**	6		
		L	66.8	1.40×10^{-5}*	2.9		X
40	Frontal Operculum Cortex	R	69.2	5.91×10^{-7}*	2.9		
		L	72.2	7.67×10^{-14}**	17		X
43	Planum Polare	R	62.4	1.43×10^{-4}*	3.3		
		L	63.4	2.94×10^{-4}*	2.5		X
46	Supracalcarine Cortex	R	66.8	8.92×10^{-7}*	2.6		
		L	80.9	4.33×10^{-17}**	9.7	Opposite	
47	Occipital Pole	R	85.5	7.22×10^{-25}**	17		
		L	75.9	1.34×10^{-12}**	5.2		X
S-8	Hippocampus	R	80.6	2.71×10^{-18}**	11		
		L	75.5	7.49×10^{-19}**	3.4		X
S-18		R	79	6.84×10^{-22}**	26		